NACA RM E51H07

NACA

# RESEARCH MEMORANDUM



## DISCUSSION OF BOUNDARY-LAYER CHARACTERISTICS NEAR THE CASING OF AN AXIAL-FLOW COMPRESSOR

By Artur Mager, John J. Mahoney, and Ray E. Budinger

Lewis Flight Propulsion Laboratory
Cleveland, Ohio





NATIONAL ADVISORY COMMITTEE FOR AERONAUTICS

WASHINGTON
December 12, 1951

NATIONAL ADVISORY COMMITTEE FOR AERONAUTICS

RESEARCH MEMORANDUM

# DISCUSSION OF BOUNDARY-LAYER CHARACTERISTICS NEAR THE CASING OF AN AXIAL-FLOW COMPRESSOR

By Artur Mager, John J. Mahoney, and Ray E. Budinger

## SUMMARY

The boundary-layer velocity profiles on the casing of an axial-flow compressor behind the guide vanes and behind the rotor were measured by use of total-pressure and claw-type yaw probes. These velocities were resolved into two components: (1) along the streamline of the flow outside the boundary layer, and (2) perpendicular to it. The affinity among all profiles was thus demonstrated with the boundary-layer thickness and the deflection of the boundary layer at the wall as the generalizing parameters. By use of these results and the momentum-integral equations, boundary-layer characteristics on the walls of an axial-flow compressor were qualitatively evaluated.

The important parameters concerning the secondary flow in the boundary layer are shown to be the turning of the flow and the product of the curvature of the streamline outside the boundary layer and the boundary-layer thickness.

Finite tip clearance is shown to affect the secondary flow primarily at high weight flows and high speeds.

The losses near the tip of the rotor blades and near the hub of the stator blades are traced to the predominantly tangential direction of the flow in the boundary layer. It is demonstrated that at large turnings the flow does not necessarily part with the surface when a separated axial velocity profile is present.

The preliminary considerations show that many of the phenomena observed in axial-flow compressors (such as relatively large losses in the rotor stages near the casing, in spite of actual energy addition to the boundary layer) are explainable when three-dimensional boundary-layer flow on the walls of the compressor is considered.

## INTRODUCTION

A large percentage of the losses through an axial compressor are concentrated in the regions immediately adjacent to the walls of the annulus (references 1 to 3). The origin of these losses has been traced by various investigators to:

(a) skin friction losses on the walls

(b) secondary flows resulting in vorticity being shed from the blades

(c) radial displacement of the boundary layer over the blade surfaces

(d) tip clearance effects

It was also noted that the decrease of axial velocity next to the annulus walls, which accompanies these losses, forces the stators and rotors to operate at angles of attack higher than design values; low lift-drag ratios thus result.

These effects, when considered separately, are known to increase the losses in axial compressors; however, the relative magnitude and significance of each effect has not been precisely determined. Some attempts to separate the various losses have been made (see reference 4) and a system which accounted for these losses in an arbitrary manner has been established (reference 1). It was next necessary to examine the process through which these losses take place simultaneously, so that steps could be taken toward their reduction. Skin-friction losses failed to account for the variation in the magnitude of the losses from stage to stage, when the boundary layer on the walls was treated similarly to an entrance section of a pipe, although the over-all boundary-layer growth was approximately equivalent (reference 3). Similarly, it became apparent that the tip-clearance effects alone could not be the chief mechanism for these losses since the losses persisted even for compressors with very small tip clearances. The large loss areas were then thought to be primarily due to secondary flows and the centrifugation of the boundary layer.

A quantitative investigation of secondary flows has been attempted first, largely because of the existence of analytical methods based on the image system of vortices (references 5 and 6). Although these methods gave fairly good qualitative answers, certain effects predicted in relation to flow direction behind cascades were exactly opposite from those actually measured. An explanation of this phenomenon was usually given in terms of large induced velocities (reference 7), which

could actually be observed, but since the method required a priori the existence of rolled-up trailing vortices (so that the induced velocities could be created), some doubt about its validity remained. In addition, since the magnitude of the centrifugal effects on the boundary layer over the blades was unknown, and since these effects theoretically must exist, further question on the validity of the secondary flow approach has arisen.

Recently, however, it became apparent that, at least in compressors designed for little or no radial flow, the effects of centrifugation must be small. The radial deflection of the boundary layer in the absence of radial flow outside the boundary layer is shown (reference 8) to depend on the ratio of the component of the rotational velocity perpendicular to the blade surface to the local velocity along the streamline and outside the boundary layer. Accordingly, the effects may be expected to be of the same order of magnitude on the pressure surface as on the suction surface of the blade. The chemical traces, which were used to show the direction of the boundary-layer flow, almost always indicated strong deflections on the suction surface and practically no deflection on the pressure surface for all compressor designs investigated.

For the most part, therefore, the observed boundary-layer deflections must be due to forces other than the centrifugal forces on the blade. Appreciable centrifugal force may nevertheless exist in some cases, but the process through which the observed boundary-layer deflections take place must depend principally on effects other than centrifugation of the boundary layer. Similar conclusions were reached by Carter (reference 7) on the basis of experiments and by Fogarty (reference 9) on the basis of actual computations of laminar boundary-layer flow over a rotating slender infinite blade.

Recently it has been shown by Squire and Winter (reference 10) and Hawthorne (reference 11) that in the case of thick boundary layers and turning, a redistribution of vorticity takes place, such that the ratio of the component of vorticity in the direction of flow to the initial vorticity is directly proportional to the turning. A mechanism for secondary flows was thereby provided that was independent of the existence of rolled-up trailing vortices. The indication was then that the losses may occur because of secondary flows, which in turn occur because of the redistribution of vorticity due to turning.

A logical step from here was to investigate three-dimensional boundary-layer characteristics on the walls of the compressor. This study was facilitated by the flow equations presented in reference 8. In order to apply these equations the velocity profiles in the boundary layer must be known. Velocity profiles on the casing of a single-stage axial compressor were measured at the NACA Lewis laboratory by use of total-pressure and yaw probes. The results of this investigation, together with an interpretation of boundary-layer characteristics on axial compressor walls, are reported herein.

Because of the great complexity of the problem and mechanical difficulties, the information obtained herein is not detailed enough to permit even an approximate computation of boundary-layer characteristics on the walls of the whole compressor. Furthermore, since these results are preliminary and of a piloting nature only, certain simplifications had to be made, both in the analysis of boundary-layer flow and in the interpretation of the data. The following assumptions were therefore made: The flow was considered incompressible, with zero velocity gradient normal to the surface at the outer extremities of the boundary layer; the pressure probes were assumed to read the correct mean values, not only of turbulent fluctuations, but also of the variation due to blade rotation; and the concept of boundary-layer thickness was interpreted as the region where frictional effects were noticeable. Such regions may be quite thick and reach well into the passage.

The information obtained is still largely qualitative, although some quantitative results appear to be of the right order of magnitude. The main purpose of this report is, however, to show that many of the hitherto unexplained phenomena appear to fall into a logical and well-defined pattern when the problem is examined with regard to three-dimensional boundary-layer flow on the walls. Thus, although the picture of flow obtained by this analysis is not accurate in all details (such a picture is still somewhat difficult to grasp), the model seems to be good enough to warrant a considerably more extensive study. In addition, the investigation discloses certain design parameters, the importance of which has previously been overlooked.

## APPARATUS

Experimental data for this report were obtained from boundary-layer investigations on a 30-inch-tip-diameter axial-flow compressor stage, which consisted of 40 circular-arc constant-thickness guide vanes and 29 constant-chord NACA 65-(12)-10 rotor blades (reference 12). The guide vanes imparted a wheel-type rotation, and the rotor imposed a vortex-type rotation on the air. A cross-sectional view of the compressor and inlet bellmouth is shown in figure 1, which also shows the location of the measuring instruments. For part of the investigation, a 1/8-inch spoiler consisting of a circular ring (fig. 1) was installed 1/2-inch upstream of the leading edge of the inlet guide vanes. The stationary clearance between the rotor blade tips and the compressor casing was 0.030 inch.

## INSTRUMENTATION

Compressor speed, weight flow, and inlet conditions were measured as described in reference 12. Outer-wall boundary-layer conditions were investigated at one circumferential position and axially at stations I, II, and III (fig. 1).

Station I was located approximately 1/6 rotor chord length upstream of the leading edge of the rotor blade tips. The one circumferential position at this station was chosen to deviate least from the mean flow values over three passages. In order to obtain this mean, total pressure and angle readings outside the boundary layer were averaged arithmetically. Total pressures were obtained with a survey probe of the type shown in figure 2(a). A claw-type yaw tube (fig. 2(b)) was used for flow angle measurements and a wedge-type static probe (fig. 2(c)) completed the instrumentation at this station.

The survey instruments at station II (approximately 1/4 chord length downstream of the rotor) were similar to those at station I, except for the addition of five thermocouple rakes (fig. 2(d)). A temperature gradient across the free-stream passage was determined from the rake readings and extrapolated to the outer wall in order to determine velocities in the boundary layer.

At station III ($1\frac{1}{3}$ chord lengths downstream of the rotor blades), the instrumentation was similar to that used at station II.

All instruments were calibrated in a steady-flow tunnel as described in reference 11. On the basis of this calibration, the accuracy of measurements is estimated as follows: static pressure, ±2.0 percent of dynamic head; total pressure, ±1.0 percent of dynamic head; and air angle, $\pm 1^{\circ}$.

Attention is called to the fact that estimates of accuracy based on the calibration in a steady-flow tunnel are not strictly applicable to the present investigation and are included only as an indication of the quality of instruments. It may be mentioned, however, that the obtained readings were easily reproducible and it was presumed that, because of the small size of instruments as compared with the pitch of the blading and the diameter of the compressor, the readings were not appreciably affected by circumferential gradients or the curvature of the wall.

## OPERATIONAL AND ANALYTICAL PROCEDURE

Outer-wall boundary-layer investigations were conducted at the design rotor speed of 840 feet per second over a range of weight flows from the upper limit (reference 11) to a flow at which stall occurred across most of the blades.

Initial tests were made with no spoiler, and the entire procedure was repeated with the 1/8-inch spoiler installed in place. Additional surveys were made at 60 percent of design speed. In this report, however, the presentation of data is limited to the velocity profiles corresponding to the following three weight flows only: the weight flow at which the maximum efficiency (of the whole compressor) occurs, and the highest and lowest weight flow for any speed. The exact values of the important parameters and the symbols designating each survey are shown in table I.

The extent of the boundary layer has been determined by plotting the measured angle and velocity against the radial position. Outside the boundary layer, the variation was small and almost linear. Near the walls, however, pronounced changes could be observed, usually with especially clear demarkation in the character of the changes in directional readings. Consequently, in order to establish the boundary-layer thickness $\delta$, the flow angle was plotted against the distance from the wall $y$. The boundary-layer thickness was determined from this plot (fig. 3) at the value of $y$ where the slope of the flow-angle curve starts increasing at a different rate.

The value of the measured angle at the position closest to the wall was considered always indicative of boundary-layer deflections there, although the velocities at this position were usually not zero. The readings of the velocity at the wall were disregarded and all curves were drawn as culminating at the zero value.

## VELOCITY PROFILES ON CASING OF COMPRESSOR

General explanation of coordinate system and parameters employed. - The momentum-integral equations developed in reference 8 (see also appendix A, equations (A1) and (A2)) are applicable to three-dimensional boundary-layer flow over rotating or stationary surfaces. One of the main assumptions in the derivation of these equations was that in the boundary layer the velocity component in the direction perpendicular to the wall is of the order of magnitude of $\delta$ and may thus be neglected when compared with terms of order of magnitude of one. A direct result of this assumption is that the change in pressure through the boundary layer is small (of the order of magnitude of $\delta$) and can also be neglected. In order to check this assumption, static-pressure measurements were taken at all three stations. Since the greatest variation observed (at station II and low weight flows) amounted to 3 percent of the value measured at the wall, neglecting the pressure change through the boundary layer appears to be valid. Consequently, if the flow conditions outside the boundary layer are known and if the shape of the velocity

distribution in the direction perpendicular to the wall (through the boundary layer) is described approximately as some function of $y/\delta$, these equations may be integrated to give a measure of the momentum lost in the boundary layer and of the flow direction near the wall.

Inasmuch as one aim of this investigation was to provide a basis for the prescription of the boundary-layer velocity distribution so that it could be used in the momentum-integral equations, the measured velocity profiles reported herein are resolved into components according to the theory of reference 8. This theory is developed for a set of orthogonal curvilinear coordinates $x,y,z$ with the restriction that $y$ be perpendicular to the wall over which the flow takes place and $x$ be in the direction of the streamline outside the boundary layer. The corresponding velocities (always relative to the wall) are $u,v,w$.

For the particular case of the boundary-layer flow over the casing (see fig. 4), the x-axis is therefore laid out along the streamline of the absolute flow and the positive direction of the y-axis is toward the hub. The positive direction of z-axis must be chosen so as to keep the system right handed. Since the system does not rotate, all components of $\omega$ are zero.

It should be noted that in a right-handed system the angles in the zx-plane are positive from $z$ to $x$.

If the boundary-layer flow over the hub of a compressor were considered and the hub were forming one continuous surface rotating with the blades, the system would have to be applied in a slightly different manner. The x-axis would have to be matched to the relative streamline and the positive direction of the y-axis would then be toward the casing. Because this system would be rotating (with positive rotation determined by the right-hand rule), the components of $\omega$ would in general be different from zero.

By use of these coordinates, therefore, the velocity profiles at various measuring stations will be described by $G$ and $g$, functions of $y/\delta$ only (all symbols are defined in appendix B):

$$u = UG\left(\frac{y}{\delta}\right)$$

and

$$w = \epsilon\, ug\left(\frac{y}{\delta}\right)$$

where $\epsilon = \tan \alpha$, and $\alpha$ is the boundary-layer deflection angle measured from the direction of the resultant skin friction stress to the direction of flow outside the boundary layer. This angle was assumed to be correctly represented by the difference in value of the flow angle as measured at the position closest to the wall and at $y = \delta$.

It is thus seen that the additional degree of freedom existing in three-dimensional boundary layers over the two-dimensional is generalized by the use of a new parameter, boundary-layer deflection at the wall. Physically, this parameter is connected with the magnitude and sign of the velocity $w$ and is thus a direct measure of the secondary flow in boundary layers. Furthermore, since the velocity $v$ (in the direction perpendicular to the wall) is neglected, the parameter $\epsilon$ represents also the limit, at the wall, of the ratio of vorticity in the direction of the streamline to that perpendicular to the streamline. (See appendix A.) It can thus be used as a basis for comparison with somewhat different considerations of the same flow by Hawthorne (reference 11) and Squire and Winter (reference 10).

In the actual solution for these parameters, additional quantities describing the shape of $G$ and $g$ are convenient to use. These quantities $H$, $K$, $J$, $L$ are so related to $G$ and $g$ that they permit expression of all significant momentum and displacement thicknesses in terms of one; the momentum thickness in the direction of the streamline. The numerical values of these quantities may be obtained by integration of proper products of $(1-G)$, $G$, and $g$ (reference 8). The physical significance of these quantities is given by:

$$H = \frac{\delta_x^*}{\theta_x}$$

$$J = \frac{1}{\epsilon} \frac{\theta_{xz}}{\theta_x}$$

$$K = \frac{1}{\epsilon} \frac{\delta_z^*}{\theta_x}$$

$$L = \frac{1}{\epsilon^2} \frac{\theta_z}{\theta_x}$$

Velocity profiles behind the guide vanes. - The velocity profiles behind the guide vanes are plotted nondimensionally against $y/\delta$ in figure 5(a). It can be seen in this figure that regardless of the weight flow, the boundary-layer thickness, the value of $\epsilon$, or the speed of

rotation, all the experimental points appear to fall fairly well on a single set of curves. A more detailed plot of the functions G and g shown in figures 5(b) and 5(c) indicates that $G = \left(\frac{y}{\delta}\right)^{\frac{1}{n}}$ and $g = \left(1 - \frac{y}{\delta}\right)^{m}$ with $n \sim 9$ and $m \sim 2$. The larger scatter of points in figure 5(c) at small values of $\left(1 - \frac{y}{\delta}\right)$ is undoubtedly due to the fact that for a fixed error in a yaw tube reading, the accuracy with which g can be determined decreases as $y \longrightarrow \delta$, since the direction of the flow in the boundary layer approaches that in the free stream.

For $n = 9$ and $m = 2$, the integrations necessary for the determination of H, K, J, L may be performed analytically (reference 8) to yield

$$H = 1.22$$

$$J = 0.556$$

$$K = 3.35$$

$$L = 1.52$$

It is thus seen that for the cases investigated the profiles behind the guide vanes on the casing of an axial-flow compressor are very similar to those obtained in an ordinary curved duct (as shown in reference 8) and are practically unaffected by the rotation of the rotor blades.

Velocity profiles behind the rotor. - The discussion and interpretation of the measurements behind the rotor blades are somewhat more complicated than in the guide vanes. This complication arises because the velocity in the boundary layer is considered relative to the casing, which is fixed, while the rotor blades exercise their effect on the flow through rotation. In order to avoid the difficulties connected with an unsteady flow, which could only be properly measured by means of instruments having an instantaneous response, a concept of a mean-force flow is introduced into this discussion. This imaginary flow is that corresponding to a system of infinitely thin blades with zero pitch and whose mean lines are such as to represent the action of the rotor and thus to affect the magnitude and direction of the mean absolute velocities outside the boundary layer. No instantaneous variations corresponding to individual blade movement exist in this concept. As a result of friction on the casing, this mean-force flow can be thought of as forming a boundary layer which is analogous to that formed in guide vanes or any curved passage. However, the velocity profiles of this

boundary layer may be affected by both the variations in the mean-force flow along the streamline outside the boundary layer and the disturbances caused by the actual presence of the rotating blades. These velocity profiles are assumed to be given correctly by fixed pressure probes behind the rotor.

The measured velocity profiles immediately behind the rotor (station II) are shown in figures 6(a) to 6(e). A study of these figures reveals that although the u-velocity profiles appear to be quite similar (except at small values of $y/\delta$), the w-velocity profiles show definite changes in form. These changes in form appear to be concentrated at low values of $y/\delta$ for the runs with the spoiler (fig. 6(d)) but extend over the whole boundary layer for the runs without the spoiler (fig. 6(b)). Moreover, when the speed is decreased to 60 percent of design value (fig. 6(e)), the differences between the profiles practically disappear.

The velocity profiles were assumed to be affected both by the changes in the mean-force flow and by the disturbances due to the presence of rotating blades; the problem of separating the effects therefore arises in an analysis of the measured profiles.

Such separation of the effects is obtained at the reduced speeds, when the disturbances tend to die out more rapidly because of low velocities. Thus the profiles obtained at 60 percent design speed may be considered as more nearly corresponding to those of the mean-force flow without additional effects due to the actual presence of the blades. A plot of these profiles on logarithmic coordinates (figs. 7(a) and 7(b)) shows that, as in guide vanes, the function $G$ is fairly closely represented by $\left(\frac{y}{\delta}\right)^{\frac{1}{n}}$, and the function $g$ varies as $\left(1 - \frac{y}{\delta}\right)^{m}$ for $n \sim 19$ and $m \sim 2$. The significant increase in the value of $n$ as compared with data obtained downstream of the guide vanes indicates that the action of the mean-force flow is such as to add energy to the boundary layer in its passage through the rotor. This phenomenon is similar to the changes occurring in two-dimensional boundary-layer profile form when the flow outside the boundary layer is accelerating. It should be realized, then, that the mean-force flow profile is considered to account for the possible variation in rotor-blade profile form and its effect on the energy addition by adjustment of the value of $n$. In other words, the value of $n$ measured in this compressor may be quite different from that measured in another compressor.

According to the preceding discussion, all deviations from $G = \left(\frac{y}{\delta}\right)^{\frac{1}{n}}$ and $g = \left(1 - \frac{y}{\delta}\right)^{m}$ are considered to be caused by the disturbances originating from the actual physical presence of the rotating

blades. A plot of G and g (figs. 7(c) and 7(d)) for the runs with the spoiler (when the initial boundary-layer thickness is large) indicates that, regardless of the weight flow, this deviation appears to be concentrated roughly within the half of the boundary layer immediately adjacent to the wall. A similar plot (figs. 7(e) to 7(h)) for runs without spoiler (when the initial boundary-layer thickness is small) shows that, although the effect for corresponding weight flows is similar, it appears to extend (especially in the case of g) over the whole boundary layer. Since the presence of the spoiler indicates a smaller value of the ratio of tip clearance to initial boundary-layer thickness than for the runs without the spoiler and since when this ratio is smaller, the deviations from the mean force profile appear to be concentrated closer to the wall, difference between the runs with and without the spoiler points to the tip clearance as the origin of the disturbances. This conclusion is not surprising, since a leakage flow from the pressure surface to the suction surface of the blade must take place and also since the tip surface of the blade drags with it some fluid, tending to reduce the relative velocity to zero.

If the mean-force velocity profile is assumed to be represented correctly by $G = \left(\frac{y}{\delta}\right)^{\frac{1}{n}}$ and $g = \left(1 - \frac{y}{\delta}\right)^{m}$, the relative component of the tip clearance flow may be obtained at any given value of $\frac{y}{\delta}$ and $\epsilon$ by use of the velocity diagram. This component is shown in figure 8(a) for the case of high weight flow. The (absolute) values of u and w in this diagram were obtained by setting $n = 19$, $m = 2$ at $y/\delta = 0.10$ and using the measured values of $\epsilon$, U, and $\beta$ for this run. The difference between the calculated and measured values of u and w is represented by $\Delta u$ and $\Delta w$. The vectorial sum of u and w then represents the assumed mean-force flow in the boundary layer, while the vectorial sum of $(u + \Delta u)$ and $(w + \Delta w)$ represents the actual flow in the boundary layer. In order to obtain these velocities in the relative sense, the tip speed is subtracted (vectorially) from the velocity U. This subtraction gives the relative direction of $u_r$. A similar subtraction is next made from the mean-force flow in the boundary layer. The resulting vector is resolved into two components: along the direction of relative U and perpendicular to it. These components are denoted by the subscript r and represent the relative values of u and w. Finally, the tip speed is subtracted from the absolute actual flow in the boundary layer. If a vector is now drawn from the relative mean-force flow to the relative actual flow, the magnitude and direction of the so postulated tip clearance flow is obtained.

A similar breakdown, at low weight flows when $\epsilon$ is increased (as follows from the actual measurements and the equations of reference 8), indicates that the tip clearance flow has increased in magnitude over that at high weight flow (fig. 8(b)). The direction of the tip clearance

flow at low weight flow is also more nearly perpendicular to the blade chord than at the high weight flow. It is thus indicated that the change in magnitude and direction of the tip clearance flow occurs because of pressure difference between the two sides of the blade. This difference is larger at low weight flow because of higher angle of attack.

The changes in shape of functions G and g are thus seen to follow a logical behavior with weight-flow variations and the origin of these changes may be traced to tip clearance flow. For compressor rotor blades in general, flows due to a finite tip clearance therefore have an adverse effect on the mean-force-flow boundary-layer profile; they cause a decrease of the u-velocity component and an increase of the w-velocity component. The decrease in the u-velocity component is more pronounced at the low weight flows, while the increase in the w-velocity component is more apparent at the high weight flows.

In view of the preceding discussion, the profile form parameters H, J, K, and L might be expected to change with speed, weight flow, and the ratio of boundary-layer thickness to tip clearance. A plot showing the values of these parameters (fig. 9) shows that although H remains almost constant, J, K, and L show large variations with weight flow. The trend of the changes in J, K, and L with weight flow is similar for the runs with or without the spoiler. At 60-percent of design speed the values of these parameters may be expected to change considerably less than at the design speed, as the plotted values show.

In order to obtain a further check on the validity of the conclusions concerning the changes in shape (due to the tip clearance) of functions, G and g, an additional set of measurements was obtained at station III, $1\frac{1}{3}$ chord length downstream of the rotor. If the changes from $G = \left(\frac{y}{\delta}\right)^{\frac{1}{n}}$ and $g = \left(1 - \frac{y}{\delta}\right)^{m}$ were caused primarily by the tip clearance flow, the effect of these disturbances should diminish downstream of the rotor and the profiles should be characterized by $G = \left(\frac{y}{\delta}\right)^{\frac{1}{n}}$ and $g = \left(1 - \frac{y}{\delta}\right)^{m}$. This effect is shown to be true regardless of weight flow or inlet boundary-layer condition (figs. 10(a) and 10(b)). Figures 10(a) and 10(b) indicate that a plausible value of n at station III is approximately 19 and that the value of m varies between 1.03 and 2.14, with most points falling on $m = 1.7$ curve.

It is thus seen that the characteristics of the flow at station III appear to confirm the previously made observations of the origin of the changes in boundary-layer profiles in passage through the rotor.

## GENERAL REMARKS ON BOUNDARY-LAYER CHARACTERISTICS IN AXIAL-FLOW COMPRESSORS

The previously discussed velocity distributions have indicated the magnitude and changes of functions G and g describing the boundary-layer profile. This information may now be utilized to obtain a very general idea about the boundary-layer characteristics in axial-flow compressors. Although the information obtained is not detailed enough to allow an accurate computation of boundary-layer growth, it should permit a somewhat more significant evaluation of important parameters and trends than hitherto obtained.

Flow near casing in region of guide vanes. - Because the velocity profiles measured downstream of the guide vanes are similar to those obtained in an ordinary curved duct, the boundary-layer equations of reference 8 should be directly applicable when the magnitude and direction of the absolute velocity outside the boundary layer are known. The procedure would be first to compute $\epsilon$ (the deflection at the wall) and then in turn to use these values of $\epsilon$ to obtain $\Theta = \theta_x R^{1/4}$, the generalized boundary-layer momentum thickness. In the computation for $\Theta$, however, an empirical constant is necessary which could not be evaluated from the measurements obtained; therefore, only speculation as to the actual growth of $\Theta$ will be attempted.

In order to obtain a general idea of the important trends, two approximate computations of $\epsilon$ are carried out by use of simplifying assumptions. First, the curvature and velocity along the streamline outside the boundary layer are assumed constant (case A, appendix A). These assumptions are very similar to those of references 10 and 11.

In addition, H and $\left(1 + \frac{1}{K - J}\right)$ are assumed to be approximately 1.0 in order to facilitate the integration. For these conditions it is shown in appendix A that the equation for $\epsilon$ reduces to:

$$\epsilon \approx \lim_{y \to 0} \frac{\xi}{\zeta} \approx - \frac{1}{2.8} \left( \frac{\Theta_o/x}{\Theta_o/x + 0.01569} + 1 \right) \beta$$

The Squire and Winter and Hawthorne solution in terms of the initial vorticity is

$$\frac{\xi}{\zeta_o} = - 2\beta$$

Although the two expressions are not exactly comparable, it is apparent that, in general, the effect of viscosity (which was neglected in references 10 and 11) as given by the approximate solution of the turbulent-boundary-layer equations is to change only the constant in the dependence of vorticity on turning.

A somewhat more significant approximate solution may be obtained with slightly different initial assumptions. If the velocity along the streamline is permitted to vary so as to satisfy the equation of continuity $U_o = U \cos \beta$, and if $c$ and $\Theta$ are assumed to have some mean constant values (the flow is along a circular arc), the equations reduce to the following form for $H = 1.0$ (see case B, appendix A):

$$\epsilon = - \frac{2}{2.764} \left( \frac{1 + \frac{c\Theta}{0.0171} \tan \beta}{\frac{0.0171}{c\Theta} + \frac{c\Theta}{0.0171}} \right) \tag{1}$$

The solution of this equation in terms of $\alpha$ is shown in figures 11(a) and 11(b) and the maximum values of $\alpha$ for any given turning are shown in figure 11(c).

It should be noted that $\epsilon$ as given by equation (1) represents an odd function, which means that a change in sign of $c$ and $\beta$ corresponds to a change in sign of $\epsilon$. Physically this means that the boundary-layer deflection at the wall will be always such as to increase the curvature of the particle path in the boundary layer over that in the free stream. Because of the approximations made in reference 8 in obtaining the solution of the boundary-layer equations, it is doubtful whether the results given in figure 11 apply for values of $\alpha$ larger than approximately $45^\circ$.

For the guide vanes used in this investigation, the measured turning was approximately $27^\circ$. The straight-line distance (chordwise) in which this turning was accomplished is estimated at 4.3 inches. The expression for curvature of a circular arc in terms of $\beta$ and chord when $\beta_o = 0$ is:

$$c = \frac{2 \sin \left( \frac{\beta}{2} \right)}{\text{chord}}$$

When the previously given values are substituted into this expression, $c = -0.108$ inch$^{-1}$. For a rough approximation of the mean value of $\Theta$, one-third the measured value at the high-weight-flow condition may be

taken. For the run without the spoiler, then, $c\Theta = -0.0029$ and with the spoiler $c\Theta = -0.0099$. For these values of $c\Theta$ and turning, the boundary-layer deflections are $7.5^\circ$ and $22.2^\circ$, respectively (see fig. 11(b)). The measured values may be obtained from table I: they are $6.8^\circ$ and $16^\circ$, respectively. Although the results obtained from the approximate solution do not agree accurately with the measured values, they are of the right order of magnitude.

It can thus be stated on the basis of figures 11(a) and 11(b) that boundary-layer deflection on the bounding walls in guide vanes (and any other similar configuration, for example, two-dimensional, stationary cascades) is primarily dependent on two parameters: the actual turning $\beta$, and the product of the generalized boundary-layer thickness $\Theta$ and the curvature of the streamline outside the boundary layer $c$.

For the range of $c\Theta$ in which guide vanes and cascades usually operate, the dependence of $\alpha$ on $c\Theta$ is practically linear and the turning acts to determine the slope of the curves.

For $c\Theta$ values larger than those usually encountered in guide vanes or cascades, a certain value of $c\Theta$ exists at which the boundary-layer deflection is maximum (see fig. 11(c)); beyond that value of $c\Theta$, the boundary-layer deflection decreases with further increase in $c\Theta$ (see fig. 11(a)). This decrease is more pronounced for small values of turning.

With respect to guide-vane design and cascade testing, these figures indicate that an increase in aspect ratio by decrease of chord alone, because of the increased curvature, may actually result in increased secondary flows in the boundary layer. The increase in curvature must, of course, be large enough to offset a possible reduction in boundary-layer thickness due to a reduced length.

Experimental evidence of this phenomenon may be found in figure 12, which is reproduced from reference 13. In this figure the ordinate represents the ratio of dynamic pressures across the cascade and can be construed as indicative of the ratio of the area blocked by secondary flow to the free area. In addition, the aspect ratio 2.0 cascade differed from the aspect ratio 1.0 cascade only in chord, while the aspect ratio 4.0 cascade differed from that of aspect ratio 1.0 only in span.

A decrease in chord is seen to result in an increase in the ratio of the areas, while the increase in span results in a decrease in the ratio of areas (fig. 12). Furthermore, the differences between the aspect ratio 2.0 and aspect ratio 1.0 cascades appear to increase somewhat with turning.

The growth of boundary-layer thickness has not yet been considered. Inasmuch as the empirical constant necessary in the computation of $\Theta$ could not be evaluated, it was impossible to compute the growth of $\Theta$ with any degree of accuracy. It can be pointed out, however, that reference 8 shows, in general, an increase of $\Theta$ with $\epsilon$. On the other hand, the difficulty with which $\epsilon$ is introduced into the equations precludes any speculation as to whether a decrease in curvature of the streamlines will decrease the generalized boundary-layer momentum thickness. In fact, for any given turning the decreased curvature of the streamlines might conceivably result in an increase in $\Theta$ because of the increase in flow-path length.

The problem of the secondary flow in the boundary layer on the bounding walls of the guide vanes or cascades has been treated in a somewhat general manner. A more detailed picture of the streamlines through the configuration (fig. 13) shows that the streamlines nearest the pressure surface for conventional compressor blades are generally almost straight and that those near the suction surface have the greatest curvature. Since the deflection in the boundary layer depends on curvature and is such, in most cases, as to increase the curvature of the particle path in the boundary layer over that in the free stream, a rough qualitative speculation may be made on the direction of the flow in the boundary layer, once the streamline paths are known. Close to the pressure surface the boundary layer should show little deflection from the direction of the streamlines. On the other hand, close to the suction surface the boundary-layer deflection should be largest and should be directed toward the actual blade surface. Because of the presence of the blade surface; the velocity perpendicular to this surface must vanish; that is, $\partial w/\partial z$ must be such that $w \rightarrow 0$ along any path adjacent to the blade surface.

Thus, whether the outer or inner wall is considered (fig. 13), $\partial w/\partial z < 0$ next to the suction surface and $\partial w/\partial z > 0$ next to the pressure surface.

Inasmuch as the continuity equation must also be satisfied (reference 8):

$$\frac{\partial w}{\partial z} = - \frac{\partial u}{\partial x} - \frac{\partial v}{\partial y} - \dot{w}_c$$

and since $\partial u/\partial x$ is generally quite small in boundary-layer flows, with $w \rightarrow 0$ at the wall, $\partial v/\partial y$ must be large (of the same order of magnitude as $\partial w/\partial z$). These considerations imply that the flow moves over the suction surface toward the midspan of the blade and over the pressure surface toward the walls. The order of magnitude of $\partial w/\partial z$ is expected to be larger near the suction surface than near the pressure

surface, because of the shape of the streamlines outside the boundary layer; larger radial flows of this type should therefore occur in the boundary layer at the suction surface. As a result of this change in direction and the friction acting over both the wall and the blade surface, a large accumulation of low-energy air may be expected in the corners between the suction surface and bounding walls. No such accumulation will occur near the pressure surface, because even if any large deflections were present close to this surface (as might happen in highly cambered blades), this deflection would, in general, be away from the blade surface. Much experimental evidence of these phenomena is available (for example, references 5, 6, and 13).

Because of small curvature of the streamlines near the pressure surface and because of the physical presence of the wall on the suction side of the passage, the deflections near both surfaces will be small (fig. 13). The largest boundary-layer flow-angle deflections may therefore be expected in the midregion of the passage, and these will be so oriented as to cause flow toward the suction surface.

Inasmuch as the losses should be at a minimum for any given turning, the preceding discussion and figure 11 indicate that, from the standpoint of secondary flows in the boundary layer, the product of streamline curvature and generalized boundary-layer momentum thickness must be kept low. High values of $c\Theta$ may perhaps be permissible only at very low turning without excessive increase of secondary boundary-layer flows.

In general, design practice is to keep the curvature as high as possible so as to reduce the axial length; inasmuch as a decrease in curvature may even result in an increase of boundary-layer thickness, the most promising way of reducing the secondary losses is apparently the reduction of boundary-layer thickness through positive means such as suction.

Flow near casing in region of rotor. - A discussion of the boundary-layer flow over that part of the casing which covers the rotor blades cannot be reduced to such simple parameters as those employed for the region near the guide vanes, even though the previously introduced concept of mean-force flow is utilized. Large changes in form parameters are caused by tip clearance effects, which are altered by speed, weight flow, and the ratio of boundary-layer thickness to tip clearance. Furthermore, in the flow through the rotor it is uncertain that the curvature of the mean-force flow streamline retains its sign. For these reasons, only very qualitative conclusions are drawn herein.

The changes in profile parameters G and g were attributed to tip clearance effects. These changes (at constant speed) were such as to increase the w-velocity profile at high weight flows and to decrease

the u-velocity profile at low weight flows. An increase in w-velocity usually signifies an increase in the secondary flows, which, for this case (as will be discussed later) means an increase in loss. The effect of tip clearance on efficiency should therefore be most pronounced at high weight flows. Inasmuch as the mean-force profile was shown to be practically unaffected by tip clearance disturbances at low speeds, the effect of tip clearance on efficiency should, in general, decrease with decrease in speed. The curves presented in figure 14, which were reproduced from reference 4, support these conclusions.

If the relative magnitude of the form factors (which are important in the determination of the deflection $\epsilon$) is considered (see fig. 9), it becomes immediately apparent that $K_T J > 0$ for all cases investigated. According to the equations for $\epsilon$, given in reference 8, therefore, $\epsilon$ will in general be of opposite sign from the curvature, when $\omega = 0$ (which is true on the nonrotating casing). Thus, the deflection of the particle paths in the boundary layer is always such as to increase its curvature over that of the mean-force flow streamline. If, however, the curvature of the mean-force flow streamline changes sign, the deflection $\epsilon$, which is obtained by a process of integration, will first decrease to zero somewhat further downstream and later reverse sign as well.

The main purpose of the guide vanes for conventional subsonic compressors is to prerotate the flow, so as to prevent compressibility effects near the tip of the first stage. As a consequence of this prerotation and the turning given to the streamlines by the rotor blades (see fig. 15), the mean-force flow streamline downstream of the rotor is curved a considerable amount away from the axial direction. In view of the discussion of $\epsilon$, which is measured toward the direction of the streamline, not only will $\epsilon$ be large (because of large turning and curvature), but also the actual direction of the flow in the boundary layer near the wall will be almost tangential. Furthermore, because of the changes in shape of the function g due to tip clearance effects, the already large w-velocity (caused by large $\epsilon$) will be even more magnified. The flow in the boundary layer near the rotor tips must therefore be largely tangential. Because of the deficiency of the axial velocity, the work done on the fluid in these regions cannot be utilized. That the work is actually done on the boundary layer flowing over the casing and near the rotor tips is evidenced by the increase in the values of n. Some of the energy added is utilized to improve the u-velocity profile, some of it is absorbed to create the secondary motion, and the rest serves to heat up the flow and the compressor. In any event, because of the axial velocity deficiency, little of the energy added ever appears as useful work. Consequently, the change in the direction of the flow in the boundary layer near the rotor tips away from axial results in a loss. It should be noted that this loss is not caused by a separation from the casing in the conventional sense where the gradient

(normal to the wall) of the velocity in the boundary layer is zero or negative at the wall. The flow in the boundary layer merely changes direction so that the axial velocity profile is separated, but the u- and w-velocity profiles show no separation whatsoever. It is shown in appendix C that the condition for an axial velocity separation is $\alpha = \pi/2 + \beta$, regardless of the shape of the u-velocity profile. In figure 16(a) the axial and tangential velocity profiles are shown for $G = (y/\delta)^{1/9}$, $g = (1 - y/\delta)^2$, $\beta = -60^\circ$, and $\alpha = 30^\circ$. This is the case for which the gradient (perpendicular to the wall) of the axial velocity is zero at the wall. When $\alpha$ is further increased to $40^\circ$ (fig. 16(b)), a definite reversal of axial velocity near the wall may be noted. Similar observations about the three-dimensional boundary-layer flow are made in reference 14, where it is noted that a separated chordwise profile does not necessarily mark the beginning of the turbulent wake for a yawed wing.

When the curvature of the streamlines outside the boundary layer changes sign, as is usually the case in the next stator row, the value of $\epsilon$ drops (and possibly also reverses sign) and causes an improvement in the axial velocity profile. A similar decrease in the value of $\epsilon$ can be seen from measurements taken at station III, where the value of $\beta$ has decreased (in the absolute sense) from that at station II because of the convergence of the passage. As may be ascertained from table I, the value of $\epsilon$ parallels the trend of $\beta$.

From this discussion, it is possible to construct the picture of boundary-layer flow over the casing and along the compressor. The direction of the streamline outside the boundary layer oscillates about the direction of the mean absolute velocity and successively assumes the values of the absolute inlet and absolute exit velocities. The deflection $\epsilon$ oscillates about the direction of the oscillating streamline in such a way that large flows in the tangential direction are caused in each rotor row, but an improvement in the axial velocity profiles is caused in the stator rows.

The large tangential flows in the rotor rows are caused primarily by the fact that the absolute turning in the rotors is toward the tangential direction and also by the tip clearance effects and the initial prerotation due to the guide vanes, which impart high absolute stagger.

For secondary boundary-layer flow on the casing, both the magnitude of the absolute turning and the direction of the mean absolute velocity have been shown to be important parameters. In addition, it appears from the equations of reference 8 that the boundary-layer thickness plays a role similar to that in the flow through guide vanes. The exact nature of the variations in $\Theta$ may not as yet be ascertained, but it is conceivable that the value of $\Theta$ may remain surprisingly small even

after quite a few compressor stages, because of the oscillation of $\epsilon$ and the energy addition in the rotors. Locally, however, the boundary-layer thickness may increase in some blade rows and decrease in others.

When the velocity w is considered in the relative sense in the rotor row (see fig. 8), it becomes apparent that this velocity is directed from the suction side of one blade to the pressure side of the adjacent blade. Furthermore, the relative magnitude is somewhat smaller than the absolute magnitude. As a consequence of this fact and in conjunction with the tip clearance, the changes in v-velocity should not be as pronounced as in the guide vane case; more important, the v-velocity should now be positive (directed toward the hub) on the pressure surface, but negative (directed toward the casing) on the suction surface. The traces of boundary-layer flow near the tip obtained in reference 15 show a very small deflection toward the hub on the pressure surface of the blades and no deflection on the suction surface. It should be noted here that all these considerations apply only in the absence of shrouding over the rotor blades. For shrouded blades, as was the case in reference 2, the streamlines outside the boundary layer must be considered in the relative sense (because the shroud rotates with the blades), which gives results similar to those discussed in the guide vanes. Near the tip a deflection would occur on the suction surface of the blade, and practically no deflection would occur on the pressure surface. These results agree with those of reference 2.

Flow near hub (unshrouded stators). - Inasmuch as the velocity profiles on the hub were not measured, this discussion can point out only the basic similarities and differences as they follow from the theory presented in reference 8. Because boundary-layer velocities are always taken relative to the surface over which the flow is passing, near the hub the whole coordinate system will rotate with the hub. Thus, the components of $\omega$ will not be zero. It has been shown (reference 8) for such cases that the change in pressure through the boundary layer is of the order of magnitude of the boundary-layer thickness. For thick boundary layers, the pressure change may be considerable and neglect of the equation of motion in the y-direction may not be justified. Should actual measurements show that ignoring this equation is justified, the streamlines outside the boundary layer (known usually as relative) must be considered (see fig. 15). These streamlines will curve away from the axial direction through the stators and toward the axial direction through the rotors. In the notation of figure 15, this statement means that the curvature will be positive through the rotors and negative through the stators. In the notation of the same figure, $\omega_y = - \omega \sin \gamma$, where $\gamma$ is the angle of inclination of the surface (see fig. 15). According to the equations for $\epsilon$, the effect of $\omega_y$ is to offset to some extent the negative curvature obtained in the stators. Large values of $\gamma$ should then be advantageous from a boundary-layer standpoint. On the other hand, the tip clearance effects in the stators will be similar to those near the tips of the rotors. As a consequence, larger losses may, in general, be expected through the stators.

The flow through the rotor row will resemble that previously discussed through the static cascade: large flows toward the tip on the suction side and little change in direction on the pressure side of the blade. Experimental evidence may again be found in traces of boundary-layer flow, as presented in references 2 and 15.

In the problem of loss reduction, aside from positive control of boundary-layer thickness $\Theta$, it may be possible to achieve some success through the control of absolute turning and of absolute mean-velocity direction. In later stages, where the compressibility effects are not great, changing the direction of the absolute mean velocity near the casing and the relative mean velocity near the hub toward axial may permit increased turning and reduce the secondary boundary-layer losses. From preliminary considerations, it appears that this end may be achieved by an increased turning near the blade roots (casing end of stators and hub end of rotors). An improvement should thereby be effected not only with respect to secondary flows in the boundary layer but also in strengthening the blades. However, a more careful evaluation of other design variables should be made before any such changes are actually attempted.

## SUMMARY OF RESULTS

The following results were obtained from experimentally obtained velocity profiles in the boundary layer on the casing of an axial compressor and from a qualitative analysis of the boundary-layer characteristics on the walls of the compressor:

1. The profiles behind the guide vanes on the casing were very similar to those obtained in an ordinary curved duct and were practically unaffected by the rotation of the rotor blades.

2. The velocity profiles behind the rotor indicated that the rotor stage adds energy to the boundary layer.

3. Flows due to a finite tip clearance for compressor rotor blades had an adverse effect on the boundary-layer profiles. The effects of tip clearance flows on the secondary flow in the boundary layer were most pronounced at high weight flows at high speeds.

4. The secondary losses in guide vanes and cascades generally were concentrated near the suction surface of the blades. In other configurations, it is important to consider whether the surface over which the boundary layer is flowing rotates integrally with the blades.

5. The losses near the tip of the rotor blades and near the hub in the stator stages occur because of the predominantly tangential direction of the boundary-layer flow near the walls.

6. The preliminary considerations indicate that a large angle of inclination of the hub surface with respect to the axis of the compressor (large hub taper) is favorable from the standpoint of secondary boundary-layer flow on the hub.

## CONCLUSIONS

The following conclusions can be drawn from the investigation:

1. The velocity profiles in the boundary layer show a definite affinity when resolved into components along the direction of the flow outside the boundary layer and perpendicular to it. The generalizing parameters are the boundary-layer thickness and the limiting deflection at the wall.

2. The important parameters concerning the secondary flow in the boundary layers are turning and $c\Theta$, where $c$ is the curvature of the streamline outside the boundary layer, and $\Theta$ is the generalized momentum thickness of the wall boundary layer. For the range of $c\Theta$ in which guide vanes and cascades usually operate, the dependence of the secondary flow on $c\Theta$ is practically linear, and turning acts to determine the slope of the curves.

3. Two types of separation may exist in a three-dimensional boundary layer. One is the conventional separation where all velocity components are separated, and the second is the directional separation, where one velocity component is separated, but others are not. Because of the directional separation, the axial velocity profile on the compressor walls may be separated in spite of the fact that the flow has not parted with the surface.

4. Although additional experimental data are necessary to improve and extend the analysis, many phenomena observed in compressors appear to be accounted for qualitatively by the method of analysis presented herein.

Lewis Flight Propulsion Laboratory
National Advisory Committee for Aeronautics
Cleveland, Ohio

## APPENDIX A

## COMPUTATION OF $\epsilon$ FOR SPECIAL CASES

The components of vorticity (reference 8) are:

$$\xi = \left[\frac{\partial w}{\partial y} - \frac{\partial v}{\partial z}\right]$$

$$\zeta = \frac{1}{1+cz}\left[\frac{\partial v}{\partial x} - \frac{\partial}{\partial y}(1 + cz)\, u\right]$$

Because of the assumptions of order of magnitude, $\frac{\partial v}{\partial x}$ and $\frac{\partial v}{\partial z}$ are neglected in boundary-layer flows when compared to $\frac{\partial u}{\partial y}$ and $\frac{\partial w}{\partial y}$, respectively. These expressions for vorticity thus reduce to:

$$\xi = \frac{\partial w}{\partial y}$$

$$\zeta = \frac{\partial u}{\partial y}$$

But by definition,

$$\epsilon = \lim_{y \to 0} \frac{\frac{\partial w}{\partial y}}{\frac{\partial u}{\partial y}}$$

thus,

$$\epsilon = \lim_{y \to 0} \frac{\xi}{\zeta}$$

The following equations from reference 8 are used to compute $\epsilon$:

$$\frac{\partial \Theta}{\partial x} + \left[\left(\frac{5H + 9}{4}\right)\frac{1}{U}\frac{\partial U}{\partial x}\right]\Theta = 0.01569 \tag{A1}$$

$$\frac{\partial \epsilon}{\partial x} + \left[\frac{4}{5}\frac{1}{\Theta}\frac{\partial \Theta}{\partial x} + \frac{9}{5}\frac{1}{U}\frac{\partial U}{\partial x} + \frac{0.01255}{K - J}\frac{1}{\Theta}\right]\epsilon = \frac{1}{J - K}\left[(1 + H)c - H\frac{2\omega_y}{U}\right] \tag{A2}$$

Substituting equation (A1) into equation (A2) gives

$$\frac{\partial \epsilon}{\partial x} + \left[0.01255\left(1 + \frac{1}{K - J}\right)\frac{1}{\Theta} - \frac{H}{U}\frac{\partial U}{\partial x}\right]\epsilon = \frac{1}{J - K}\left[(1 + H)c - H\frac{2\omega_y}{U}\right] \tag{A3}$$

This equation is solved for two special cases:

Case A. - If $\frac{\partial U}{\partial x} = 0$, c = constant, and $\omega_y = 0$, equation (A3) reduces to:

$$\frac{\partial \epsilon}{\partial x} + 0.01255\left(1 + \frac{1}{K - J}\right)\frac{\epsilon}{\Theta} = \frac{1 + H}{J - K}c \tag{A4}$$

the solution of which is:

$$\epsilon\, E(x) = \text{Constant} + \frac{1 + H}{J - K}c\int_0^x E(x)\, dx \tag{A5}$$

where

$$E(x) = \exp\left[0.01255\left(1 + \frac{1}{K - J}\right)\int_0^x \frac{dx}{\Theta}\right] \tag{A6}$$

and the boundary condition is at $x = 0$, $\epsilon = 0$, $\Theta = \Theta_o$. Thus the constant in equation (A5) is zero.

Equation (A1) is again used to evaluate equation (A6),

$$\frac{\partial\Theta}{\partial x} = 0.01569 \tag{A7}$$

and

$$E(x) = E_1(x) = \Theta^{\frac{4}{5}\left(1 + \frac{1}{K - J}\right)}$$

If it is now noted that $H \approx \frac{4}{5}\left(1 + \frac{1}{K - J}\right) \approx 1.0$ but $K - J \approx 2.8$, equation (A5) becomes:

$$\epsilon \approx - \frac{2}{2.8} \frac{c}{\Theta} \int_0^x \Theta \, dx \tag{A8}$$

and when equation (A7) is substituted,

$$\epsilon \approx - \frac{cx}{2.8}\left(\frac{\Theta_o/x}{\Theta_o/x + 0.01569} + 1\right) \tag{A9a}$$

Inasmuch as $c = \frac{d\beta}{dx}$ and at $x = 0$ $\beta_o = 0$, by definition equation (A9a) may also be written

$$\epsilon = \lim_{y \to 0} \frac{\xi}{\zeta} \approx - \frac{1}{2.8}\left(\frac{\Theta_o/x}{\Theta_o/x + 0.01569} + 1\right)\beta \tag{A9b}$$

Case B. - If $c$ = constant, $\omega_y = 0$ and $\Theta$ = constant (mean value) but $U_o = U \cos \beta$ then equation (A6) (which is not restricted to the limitations of case A) becomes:

$$E(x) = E_2(x) = \exp\left(0.0171 \frac{x}{\Theta}\right)$$

The solution of equation (A3) is now:

$$\epsilon = \frac{(1 + H)\, c}{(J - K) \cos^H \beta \, E_2(x)} \int_0^x E_2(x) \cos^H \beta \, dx \tag{A10}$$

This equation can be integrated in closed form if it is recalled that $H \approx 1.0$ and $\beta = cx$:

$$\epsilon \approx \frac{2}{J - K}\left(\frac{1 + \frac{c\Theta}{0.0171}\tan\beta}{\frac{c\Theta}{0.0171} + \frac{0.0171}{c\Theta}}\right) \tag{A11}$$

The value of $c\Theta$ at which $\epsilon$ is a maximum is found from equation (A11) by differentiation, and so forth, to be:

$$\left(c\Theta\right)_{\epsilon_{max}} = 0.0171\ Q \tag{A12}$$

where

$$Q \equiv \tan\beta \pm \sqrt{\tan^2\beta + 1}$$

The values of $\epsilon_{max}$ can now also be found:

$$\epsilon_{max} = \frac{2Q}{J - K}\left(\frac{1 + Q\tan\beta}{Q^2 + 1}\right) \tag{A13}$$

## APPENDIX B

## SYMBOLS

The following symbols are used in this report:

| | |
|---|---|
| C | rotor chord |
| c | curvature of x-axis, $d\beta/dx$ |
| G,g | functions describing boundary-layer velocity profile |
| H,J,K,L | quantities describing relations among various characteristic loss thicknesses in boundary layer |
| m | exponent in expression for g |
| n | reciprocal of exponent in expression for G |
| R | Reynolds number based on $\theta_x$, $\theta_x U/\nu$ |
| Re | Reynolds number based on rotor chord, $CU/\nu$ |
| U | velocity outside boundary layer along streamline of potential flow (relative to wall over which the flow takes place) |
| W | weight flow |
| $W_{me}$ | weight flow at maximum efficiency |
| u,v,w | time-averaged velocities in curvilinear coordinate system (relative to wall over which the flow takes place) |
| x,y,z | orthogonal curvilinear coordinate system with x along streamline of potential flow and y perpendicular to wall over which the flow takes place |
| $\alpha$ | boundary-layer deflection angle measured from direction of resultant skin-friction stress to direction of flow outside boundary layer |
| $\beta$ | angle between axial direction and tangent to x-axis (angle between axial direction and streamline outside boundary layer) |
| $\gamma$ | angle between tangent to hub surface and axis of compressor |
| $\delta$ | boundary-layer thickness |

$\delta_x^*$ displacement thickness in x-direction $\frac{1}{U}\int_0^\delta (U - u)\, dy$

$\delta_z^*$ displacement thickness in z-direction $\frac{1}{U}\int_0^\delta w\, dy$

$\epsilon$ measure of boundary-layer deflection near wall, $\tan \alpha$

$\Theta$ generalized boundary-layer momentum-loss thickness, $\theta_x R^{1/4}$

$\theta_x$ momentum thickness in x-direction of flow in x-direction

$$\frac{1}{U^2}\int_0^\delta (U - u)\, u\, dy$$

$\theta_z$ momentum thickness in z-direction of flow in z-direction

$$\frac{1}{U^2}\int_0^\delta w^2\, dy$$

$\theta_{xz}$ momentum thickness in z-direction of flow in x-direction

$$\frac{1}{U^2}\int_0^\delta (U - u)\, w\, dy$$

$\nu$ kinematic viscosity

$\xi, \zeta$ components of vorticity vector in x- and z-directions, respectively

$\tau_o$ shear stress at wall

$\omega$ angular velocity

I, II, III measuring stations

Subscripts:

a in axial direction

max maximum

| | |
|---|---|
| o | initial value |
| r | relative to blade |
| t | in tangential direction |
| y | in y-direction |

## APPENDIX C

## CONDITIONS WHEN AXIAL VELOCITY PROFILE BECOMES SEPARATED

The expression for axial velocity is:

$$u_a = u \cos \beta + w \sin \beta$$

In order to find the separation point it is necessary to investigate the conditions under which the axial velocity becomes tangential to the y-axis at the surface:

$$\left.\frac{du_a}{dy}\right]_{y=0} = \left.\frac{du}{dy}\right]_{y=0} \cos \beta + \left.\frac{dw}{dy}\right]_{y=0} \sin \beta = 0$$

But by definition

$$\lim_{y \to 0} \frac{\frac{dw}{dy}}{\frac{du}{dy}} = \epsilon = \tan \alpha$$

thus

$$\left.\frac{du_a}{dy}\right]_{y=0} = \left.\frac{du}{dy}\right]_{y=0} (\cos \beta + \epsilon \sin \beta) = 0$$

This equation is obviously satisfied regardless of the value of $\left.\frac{du}{dy}\right]_{y=0}$, when

$$\alpha = \frac{\pi}{2} + \beta$$

and the flow near the wall is tangential.

## REFERENCES

1. Howell, A. R.: Fluid Dynamics of Axial Compressors. War Emergency Issue No. 12 pub. by Inst. Mech. Eng. (London), 1945. (Reprinted in U.S. by A.S.M.E., Jan. 1947, pp. 441-452.)

2. Weske, John R.: An Investigation of the Aerodynamic Characteristics of a Rotating Axial-Flow Blade Grid. NACA TN 1128, 1947.

3. Bowen, John T., Sabersky, Rolf H., and Rannie, W. Duncan: Theoretical and Experimental Investigations of Axial Flow Compressors. Mech. Eng. Lab., Parts 1 and 2, Jan. and July 1949. (Navy Contract No. N6-ORI-102, Task Order IV.)

4. Fickert: The Influence of the Radial Clearance of the Rotor on the Compressor Efficiency, Dec. 12, 1944. Part C of The Influence of Physical Dimensions (Such as Hub:Tip Ratio, Clearance, Blade Shape) and Flow Conditions (Such as Reynolds Number and Mach Number) on Compressor Characteristics. Bur. Ships 338, Navy Dept., May 1946, pp. 95-108.

5. Lieblein, Seymour, and Ackley, Richard H.: Secondary Flows in Annular Cascades and Effects on Flow in Inlet Guide Vanes. NACA RM E51G27, 1951.

6. Carter, A. D. S., and Cohen, Elizabeth M.: Preliminary Investigation into the Three-dimensional Flow through a Cascade of Aerofoils. R.& M. No. 2339, British A.R.C., Feb. 1946.

7. Carter, A. D. S.: Three-dimensional-flow Theories for Axial Compressors and Turbines. War Emergency Issue No. 41 pub. by Inst. Mech. Eng. (London). (Reprinted in U.S. by A.S.M.E., April 1949, pp. 255-268.)

8. Mager, Artur: Generalization of Boundary-Layer Momentum-Integral Equations to Three-Dimensional Flows Including Those of Rotating System. NACA TN 2310, 1951.

9. Fogarty, Laurence Eugene: The Laminar Boundary Layer on a Rotating Blade. Jour. Aero. Sci., vol. 18, no. 4, April 1951, pp. 247-252.

10. Squire, H. B., and Winter, K. G.: The Secondary Flow in a Cascade of Airfoils in a Nonuniform Stream. Jour. Aero. Sci., vol. 18, no. 4, April 1951, pp. 271-277.

11. Hawthorne, William R.: Secondary Circulation in Fluid Flow. Gas Turbine Lab., M.I.T., May 1950.

12. Mahoney, John J., Dugan, Paul D., Budinger, Raymond E., and Goelzer, H. Fred: Investigation of Blade-Row Flow Distributions in Axial-Flow-Compressor Stage Consisting of Guide Vanes and Rotor-Blade Row. NACA RM E50G12, 1950.

13. Erwin, John R., and Emery, James C.: Effect of Tunnel Configuration and Testing Technique on Cascade Performance. NACA TN 2028, 1950.

14. Kuethe, A. M., McKee, P. B., and Curry, W. H.: Measurements in the Boundary Layer of a Yawed Wing. NACA TN 1946, 1949.

15. Ruden, P.: Untersuchungen über einstufige Axialgebläse. Luftfahrtforschung, Bd. 14, Lfg. 7, July 20, 1937, S. 325-346. (Available as NACA Technical Memorandum 1062.)

TABLE I - SUMMARY OF EXPERIMENTAL CONDITIONS

| Symbol | | ◹ | ▽ | ◸ | △ | ○ | □ | ◇ | ▷ |
|---|---|---|---|---|---|---|---|---|---|
| Design speed (percent) | | 100 | 100 | 100 | 100 | 100 | 100 | 60 | 60 |
| Corrected weight flow, (lb/sec)* | | 59.9 | 51.6 | 38.8 | 59.3 | 51.8 | 41.7 | 35.7 | 28.6 |
| Efficiency | | 0.796 | 0.898 | 0.786 | 0.785 | 0.885 | 0.833 | 0.878 | 0.885 |
| Spoiler thickness (in.) | | 0 | 0 | 0 | 1/8 | 1/8 | 1/8 | 0 | 0 |
| Station I | $\delta$ (in.) | 0.180 | 0.200 | 0.290 | 0.350 | 0.400 | 0.450 | 0.200 | 0.200 |
| | $\beta$ (deg) | 26.7 | 27.2 | 29.0 | 26.1 | 26.1 | 27.5 | 25.9 | 26.6 |
| | U (ft/sec) | 560 | 466 | 325 | 558 | 469 | 354 | 309 | 247 |
| | $\alpha$ (deg) | 6.6 | 6.8 | 14.6 | 16.4 | 16.0 | 19.2 | 8.5 | 9.0 |
| | $\epsilon$ | 0.115 | 0.120 | 0.261 | 0.294 | 0.287 | 0.349 | 0.149 | 0.095 |
| | $\Theta$ (in.) | 0.081 | 0.104 | 0.149 | 0.275 | 0.286 | 0.344 | 0.073 | 0.108 |
| | $Re \times 10^{-4}$ | 60.0 | 52.5 | 37.7 | 59.6 | 52.1 | 40.0 | 35.3 | 28.6 |
| Station II | $\delta$ (in.) | 0.610 | 0.780 | 1.320 | 0.780 | 0.800 | 1.320 | 0.528 | 0.780 |
| | $\beta$ (deg) | 41.9 | 52.4 | 60.1 | 41.6 | 51.4 | 56.3 | 44.5 | 53.5 |
| | U (ft/sec) | 689 | 680 | 659 | 696 | 675 | 657 | 412 | 394 |
| | $\alpha$ (deg) | 11.6 | 14.4 | 25.0 | 15.5 | 15.1 | 30.2 | 13.1 | 14.6 |
| | $\epsilon$ | 0.206 | 0.257 | 0.467 | 0.277 | 0.269 | 0.583 | 0.233 | 0.260 |
| | $\Theta$ (in.) | 0.304 | 0.271 | 0.859 | 0.524 | 0.358 | 0.852 | 0.208 | 0.261 |
| | $Re \times 10^{-4}$ | 76.1 | 81.5 | 78.0 | 76.1 | 79.7 | 77.7 | 48.0 | 46.6 |
| Station III | $\delta$ (in.) | 0.684 | 1.15 | 0.950 | 0.684 | 0.820 | 1.39 | ---- | ---- |
| | $\beta$ (deg) | 37.3 | 45.7 | 57.8 | 38.3 | 47.0 | 53.1 | ---- | ---- |
| | U (ft/sec) | 764 | 702 | 612 | 751 | 687 | 655 | ---- | ---- |
| | $\alpha$ (deg) | 7.9 | 9.0 | 13.7 | 8.1 | 8.1 | 16.0 | ---- | ---- |
| | $\epsilon$ | 0.139 | 0.158 | 0.243 | 0.142 | 0.143 | 0.287 | ---- | ---- |
| | $\Theta$ (in.) | 0.341 | 0.301 | 0.435 | 0.325 | 0.425 | 1.215 | ---- | ---- |
| | $Re \times 10^{-4}$ | 84.0 | 83.2 | 73.2 | 82.6 | 89.1 | 79.4 | ---- | ---- |

*To standard conditions.

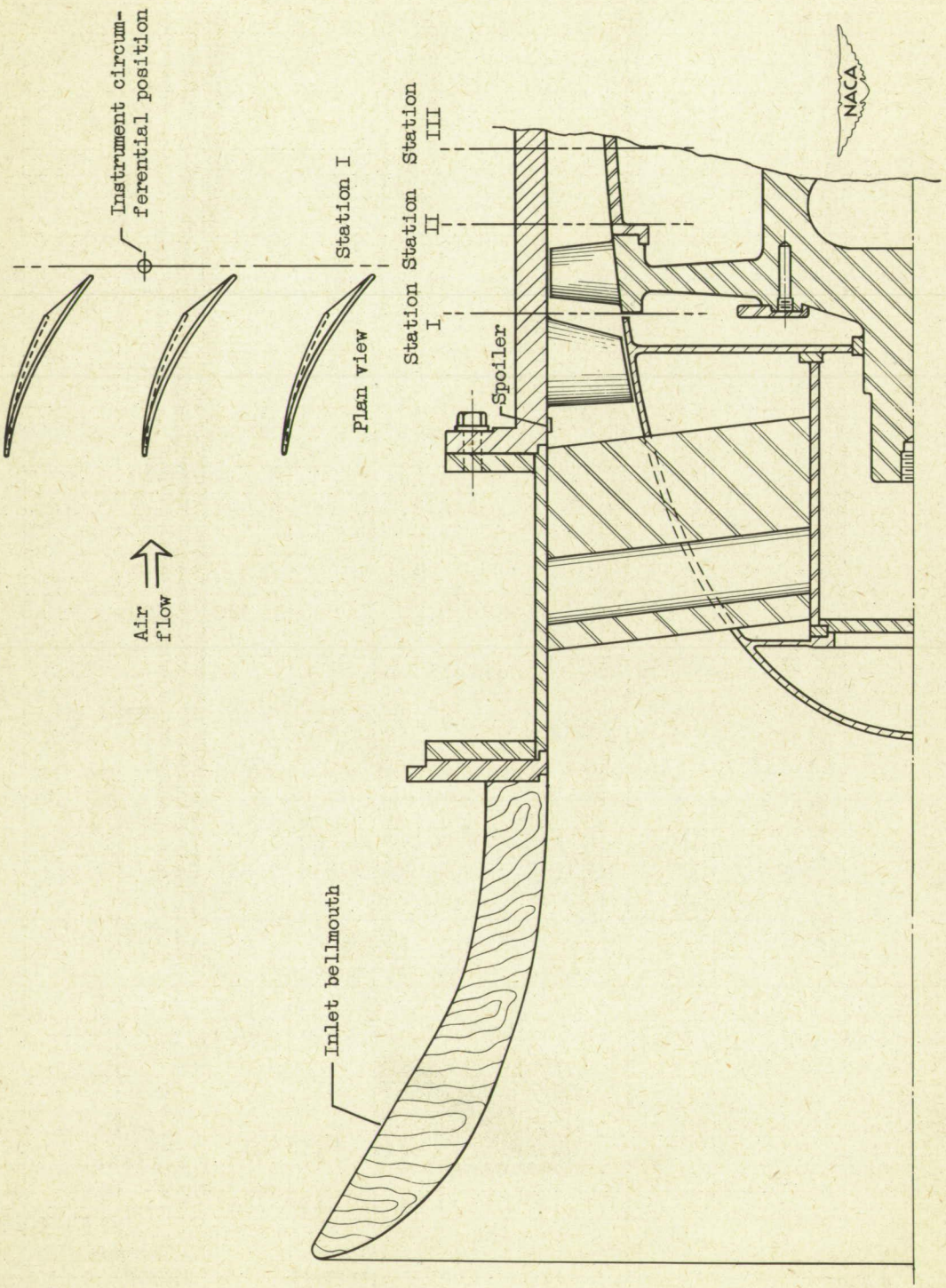


Figure 1. - Cross-sectional view of compressor showing instrument locations.

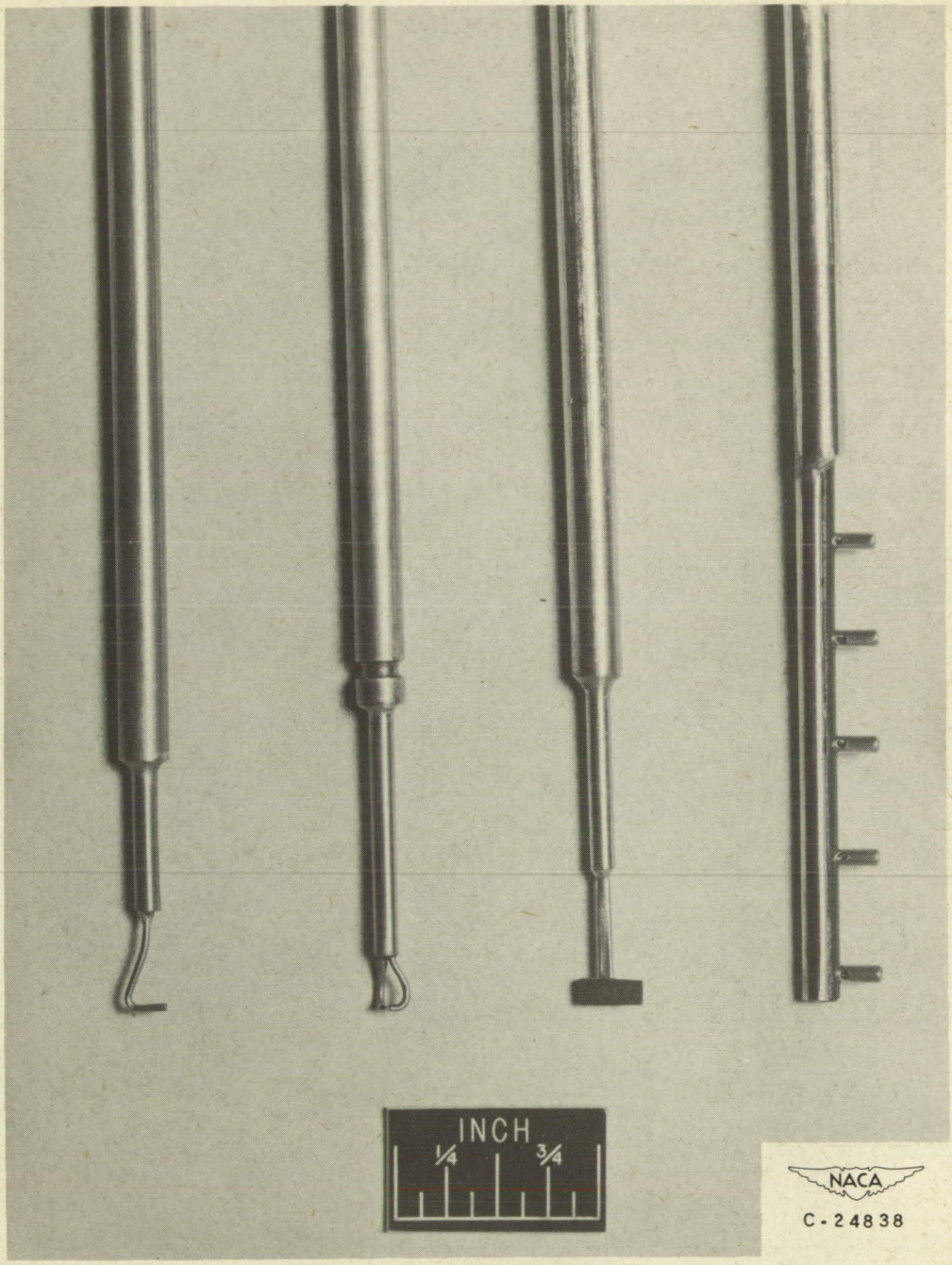


(a) Total-pressure survey probe. (b) Claw-type yaw tube. (c) Wedge-type static-pressure survey probe. (d) Thermocouple rake.

Figure 2. - Instruments.

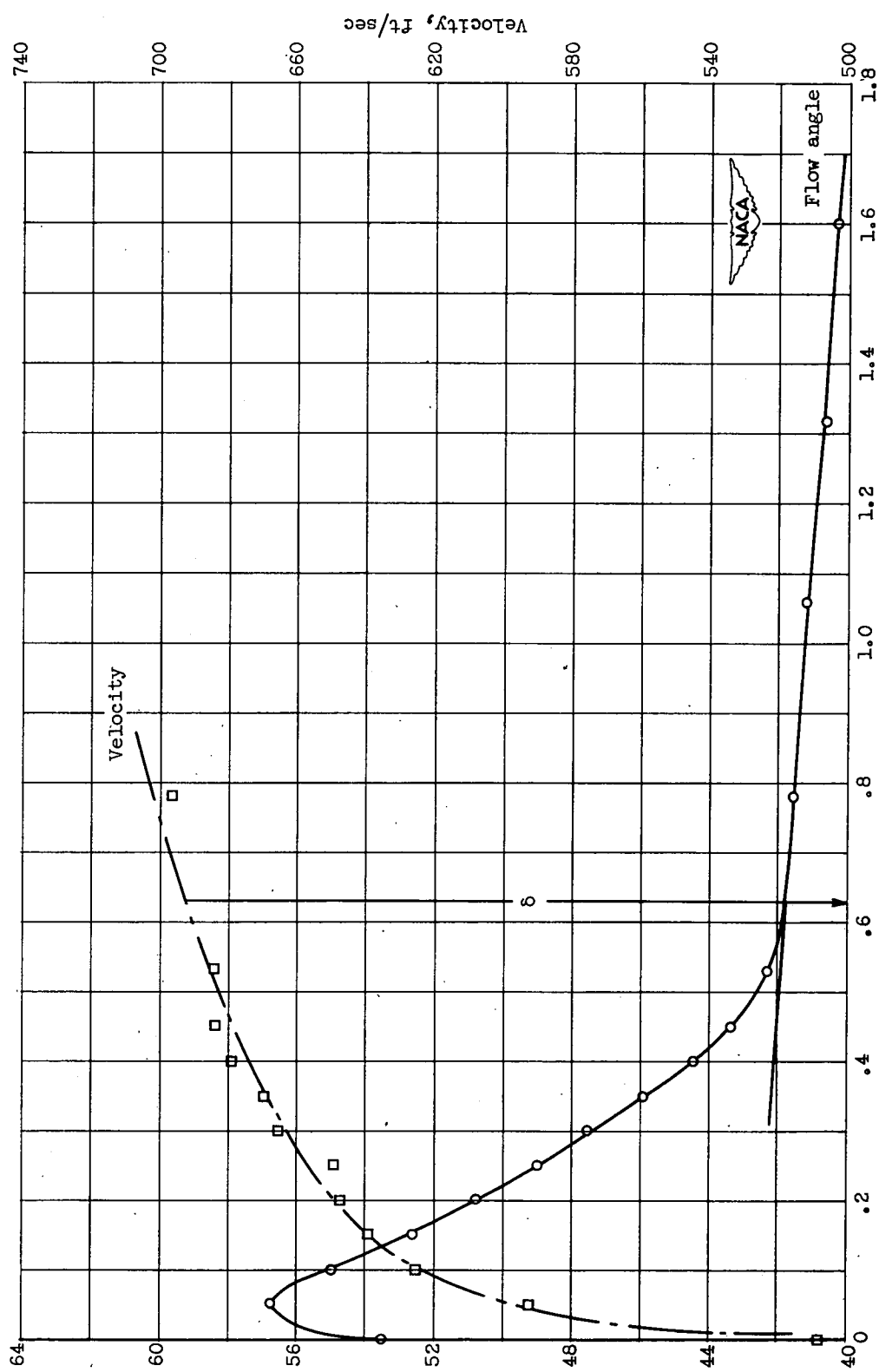


Figure 3. - Determination of boundary-layer thickness δ.

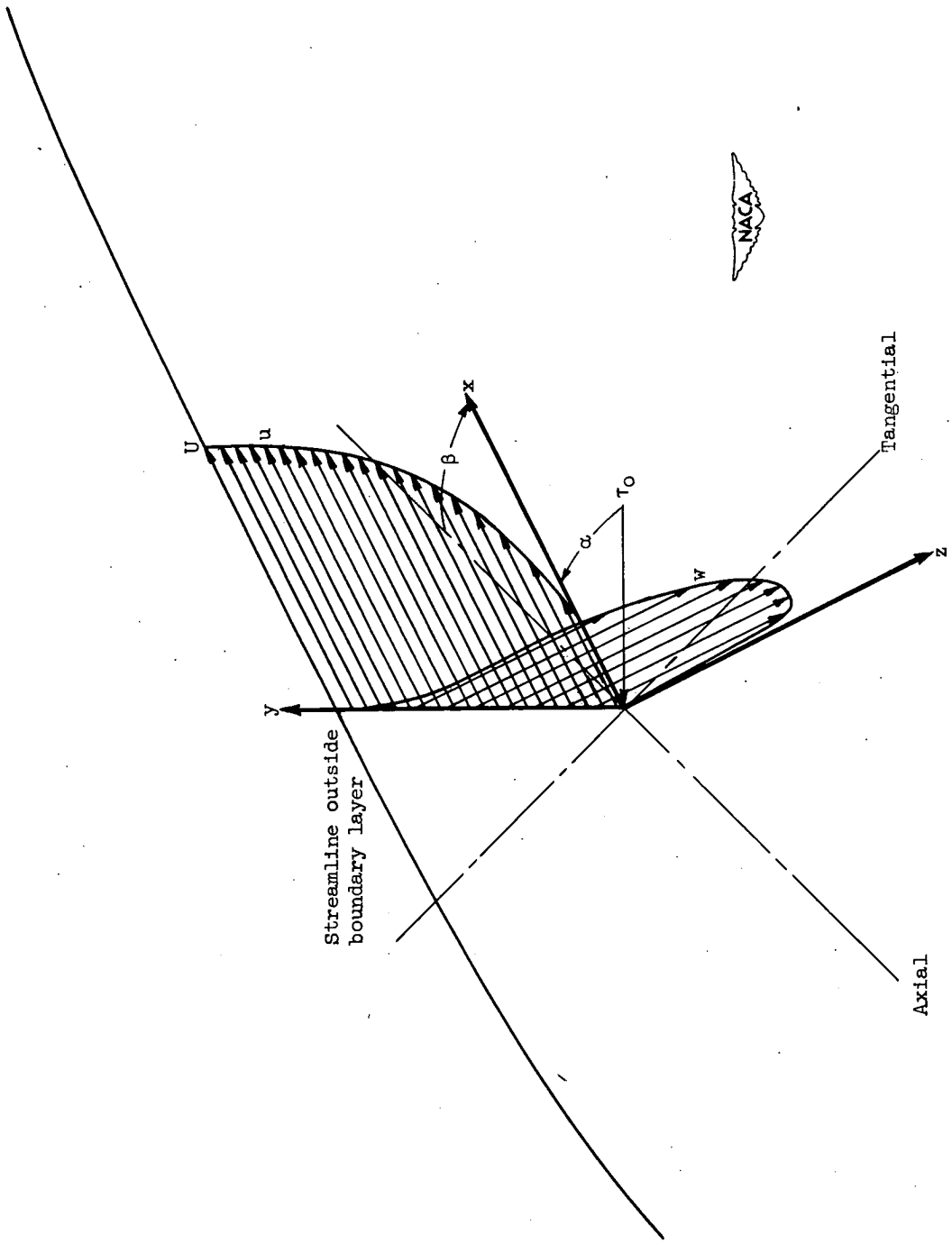


Figure 4. - Coordinate system used in analysis of boundary-layer velocity profiles.

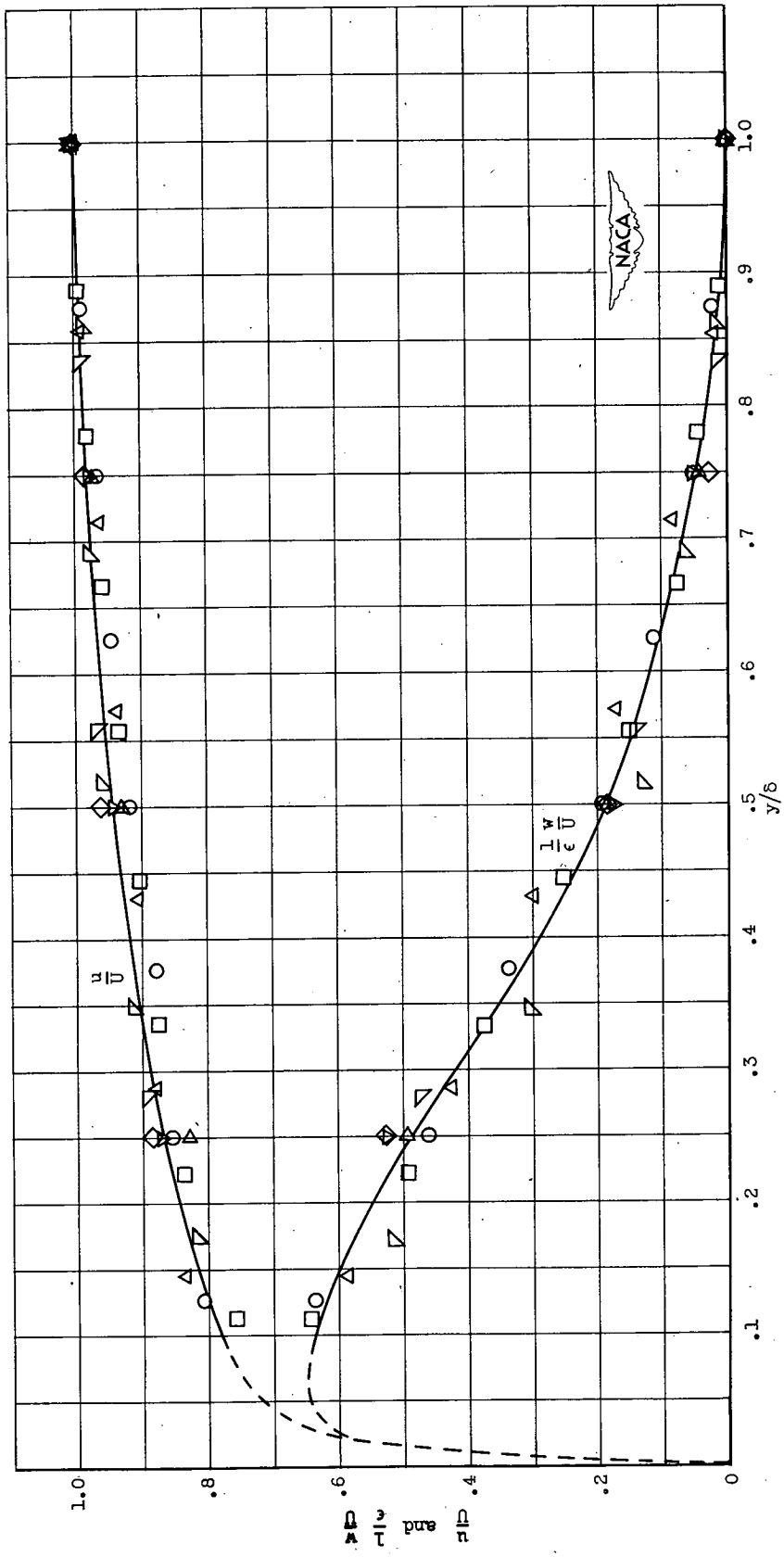


(a) Velocities $\frac{u}{U}$ and $\frac{w}{U}\frac{1}{\epsilon}$.

Figure 5. - Velocity profiles downstream of guide vanes. (See table I for explanation of data points.)

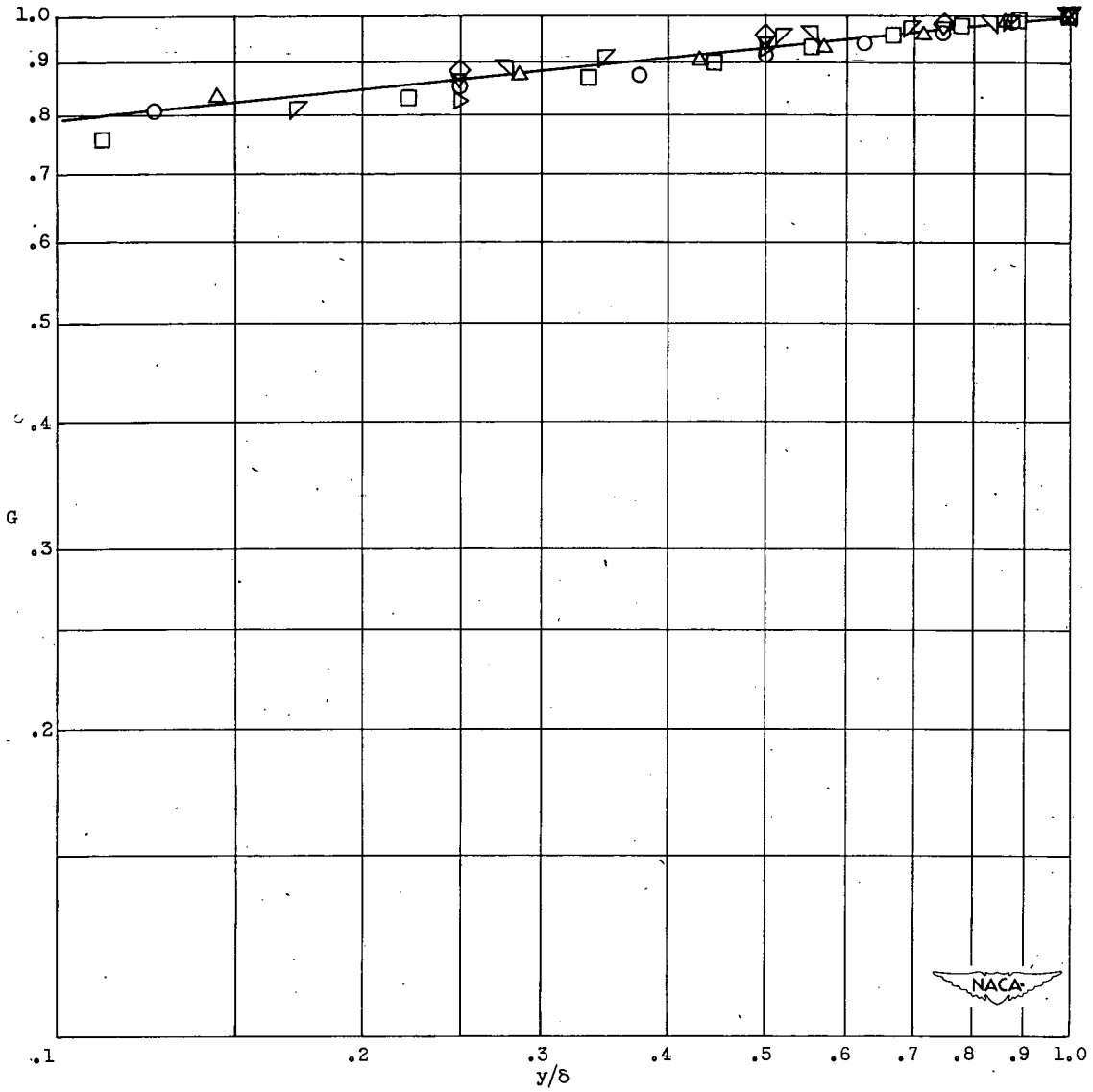


(b) Function G.

Figure 5. - Continued. Velocity profiles downstream of guide vanes. (See table I for explanation of data points.)

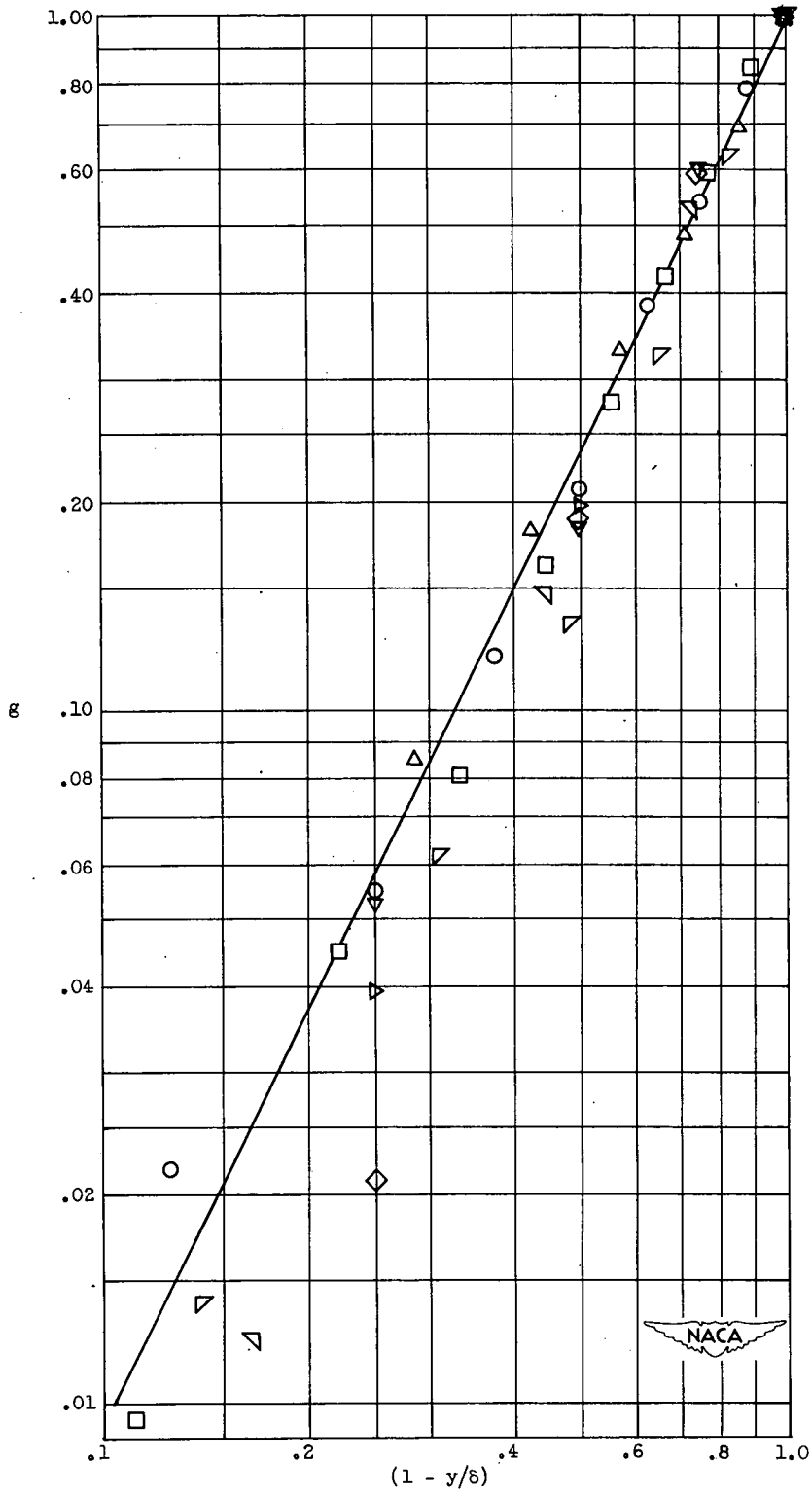


(c) Function g.

Figure 5. - Concluded. Velocity profiles downstream of guide vanes. (See table I for explanation of data points.)

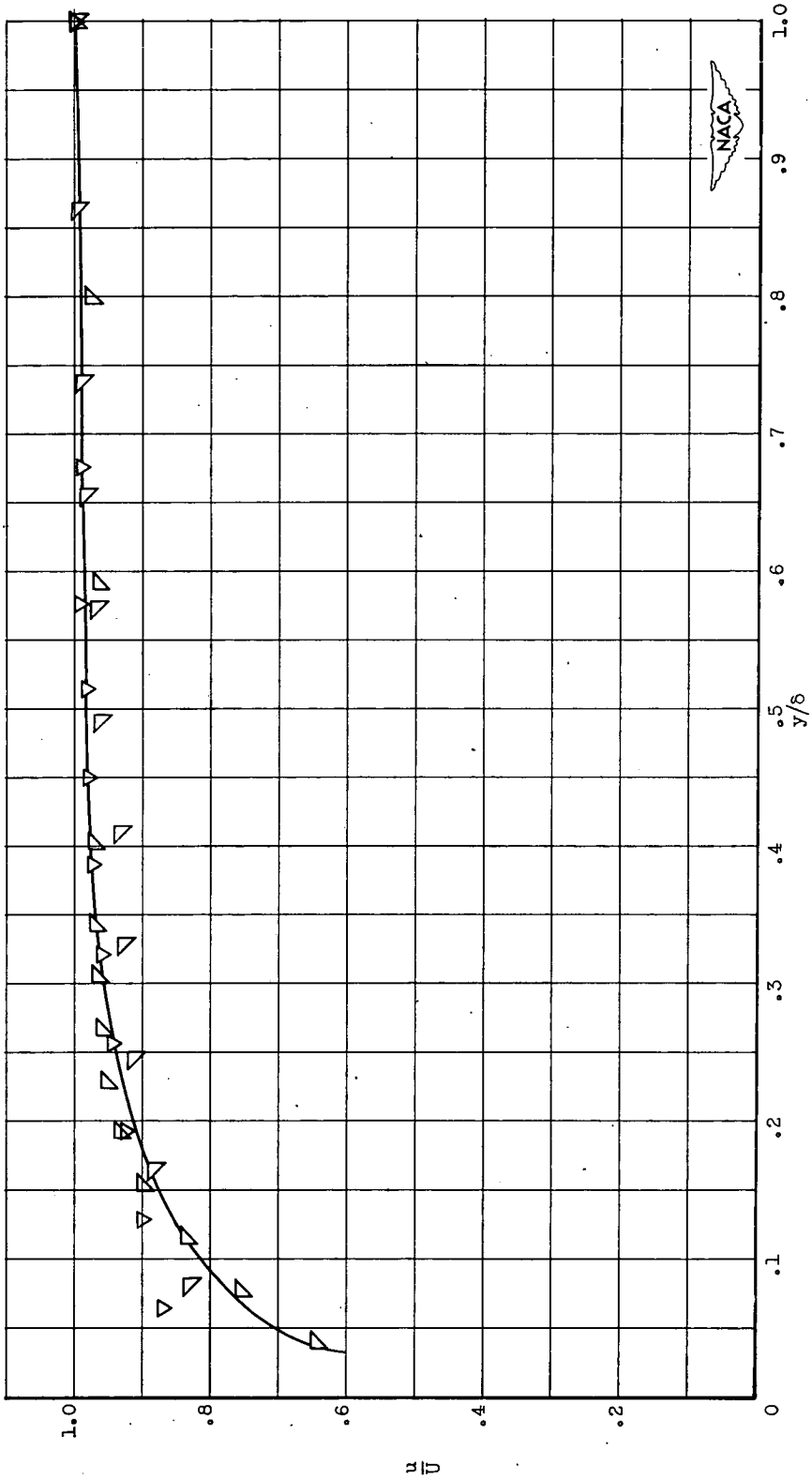


(a) Velocity $\frac{u}{U}$; no spoiler.

Figure 6. - Velocity profiles downstream of rotor (station II). (See table I for explanation of data points.)

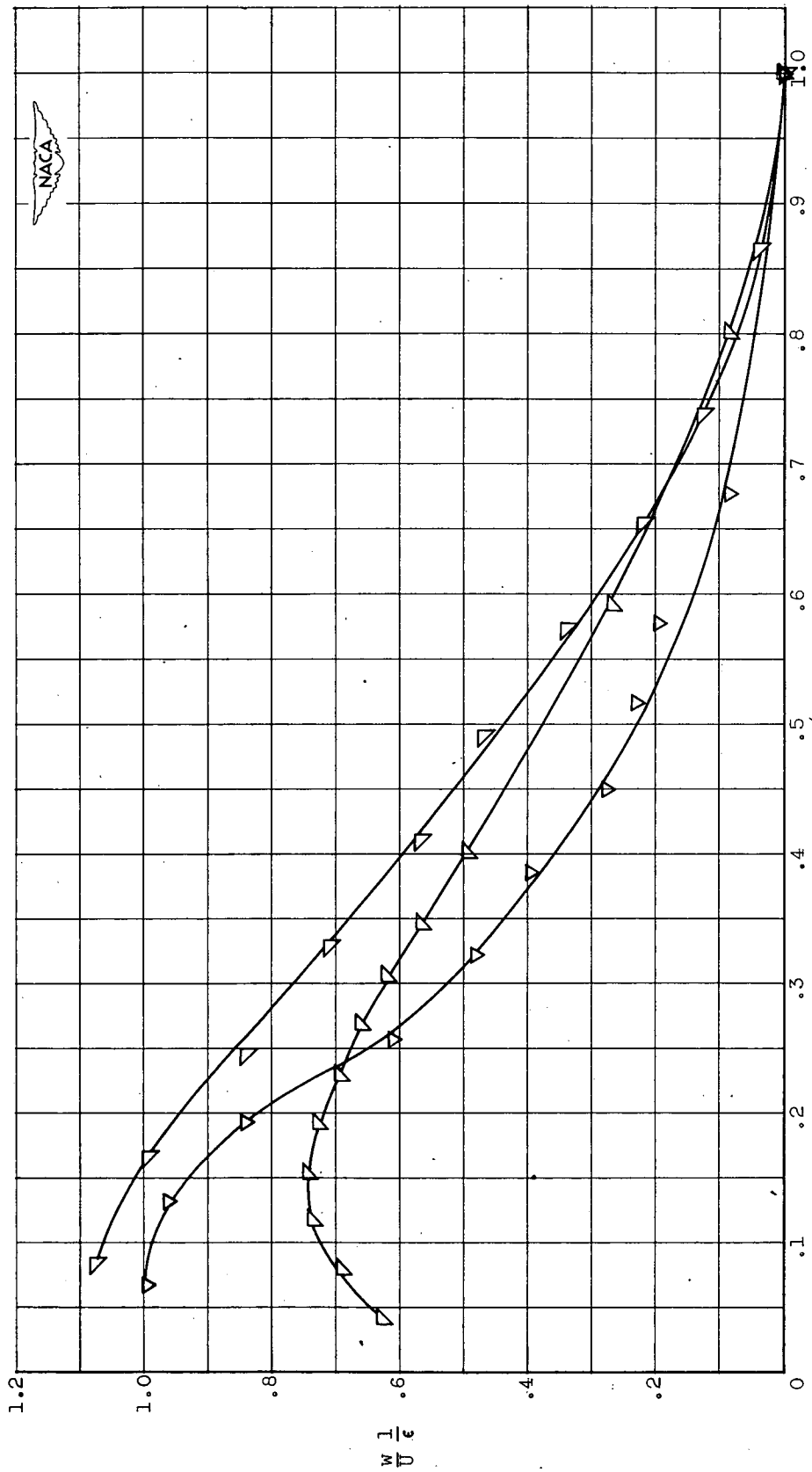


(b) Velocity $\frac{w}{U}\frac{1}{\epsilon}$; no spoiler.

Figure 6. - Continued. Velocity profiles downstream of rotor (station II). (See table I for explanation of data points.)

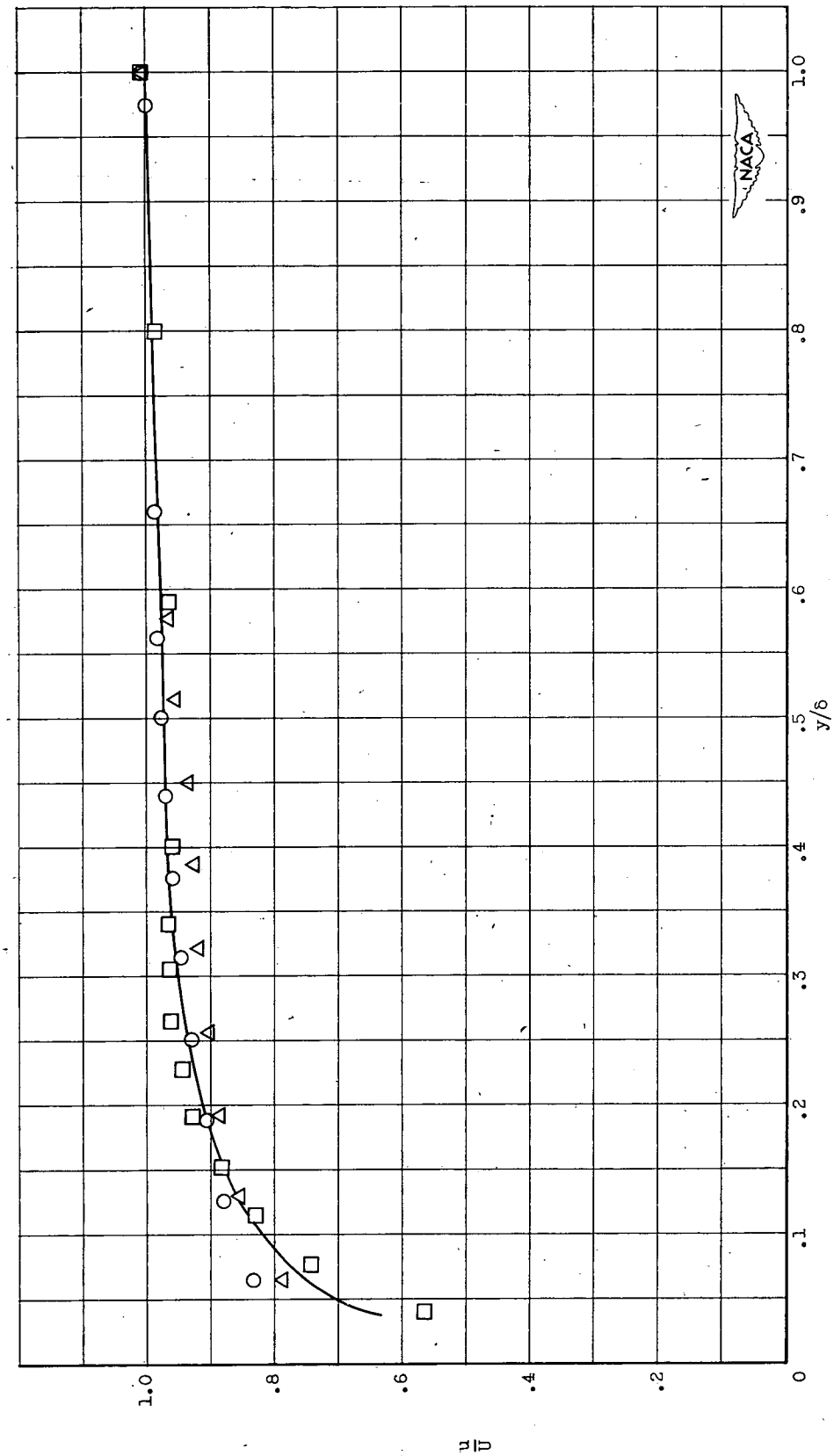


(c) Velocity $\frac{u}{U}$; $\frac{1}{8}$-inch spoiler.

Figure 6. - Continued. Velocity profiles downstream of rotor (station II). (See table I for explanation of data points.)

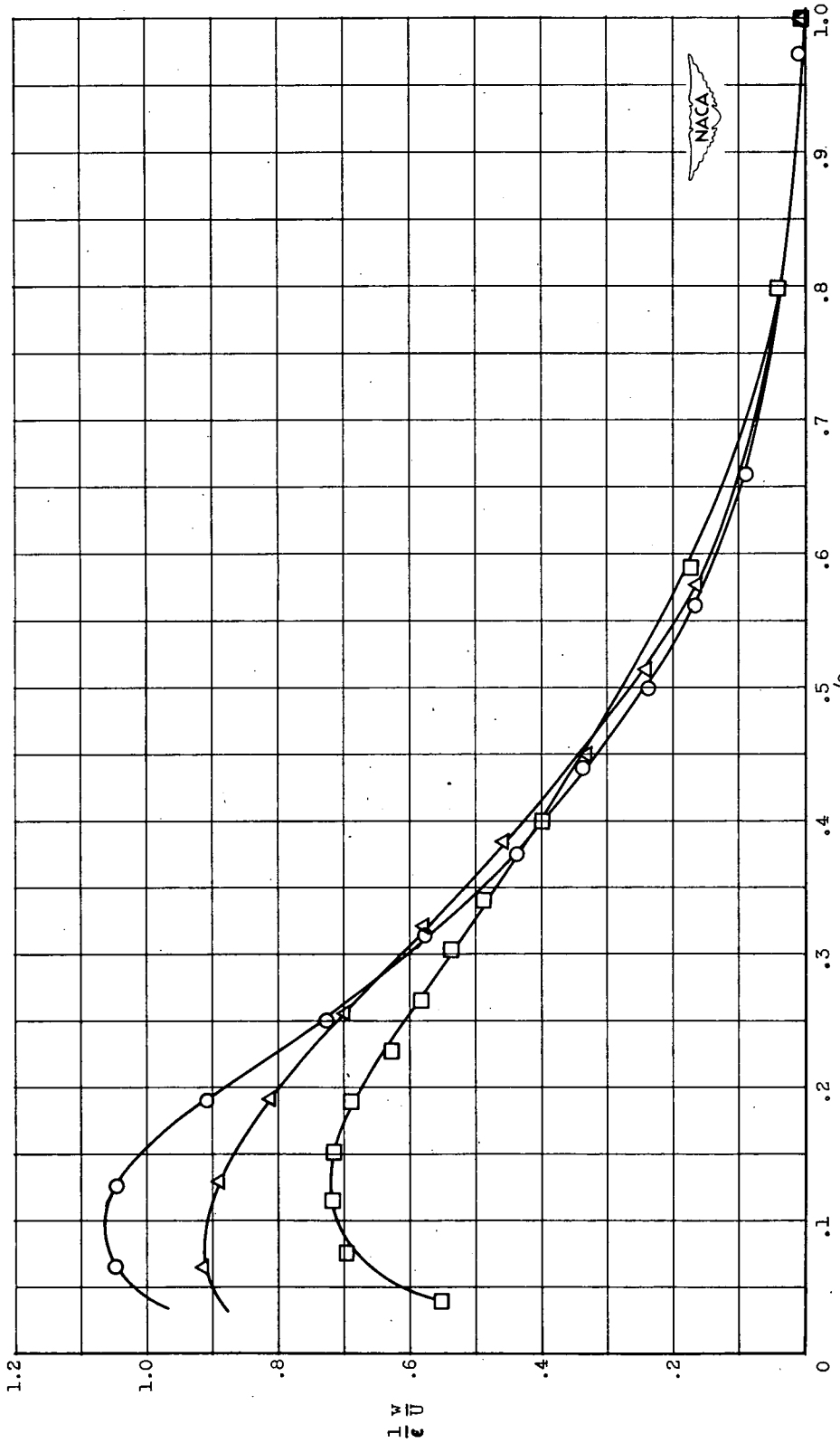


(d) Velocity $\frac{w}{U}\frac{1}{\epsilon}$; $\frac{1}{8}$-inch spoiler.

Figure 6. - Continued. Velocity profiles downstream of rotor (station II). (See table I for explanation of data points.)

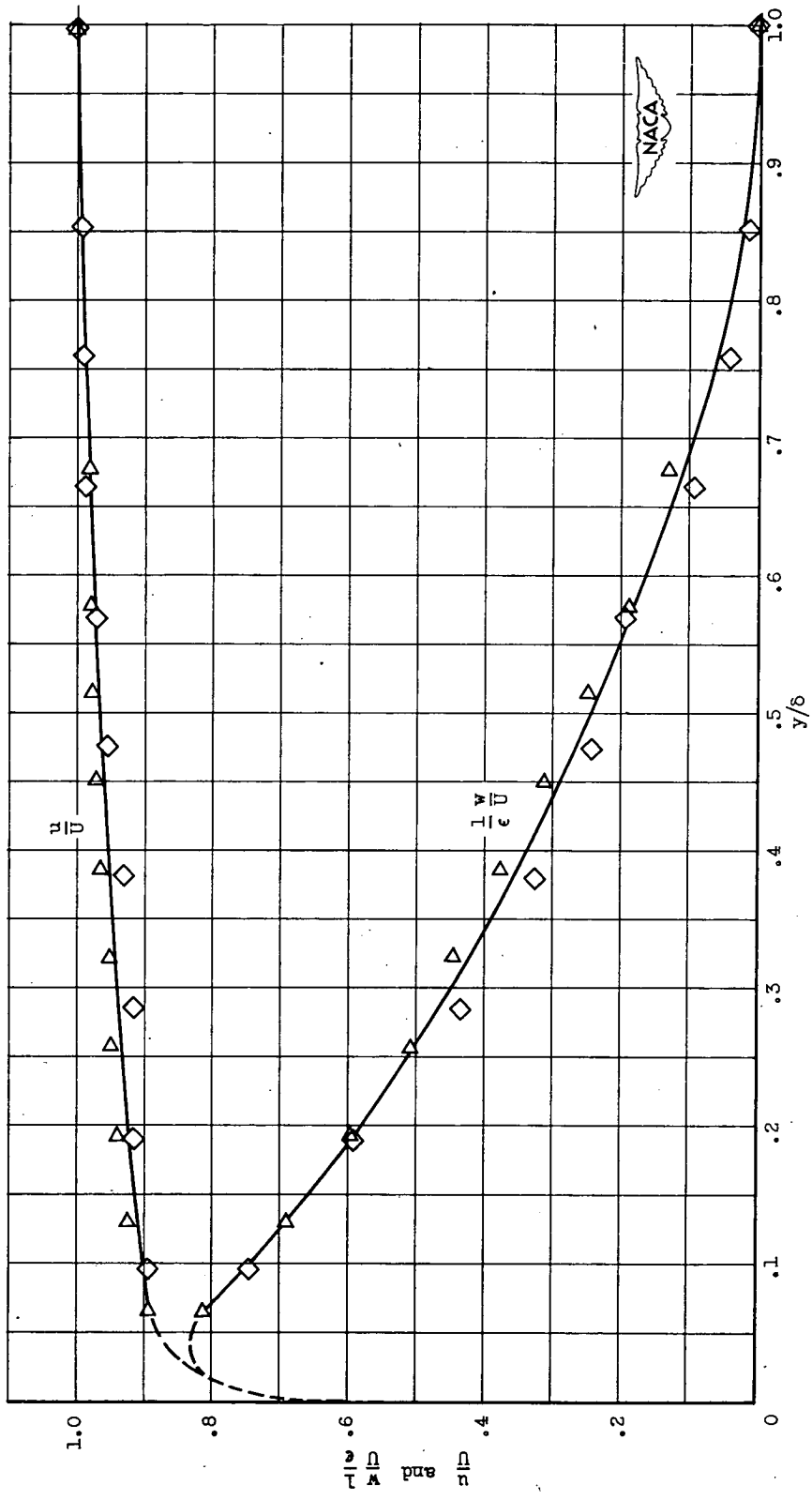


(e) Velocities $\frac{u}{U}$ and $\frac{1}{\epsilon}\frac{w}{U}$; no spoiler; 60 percent of design speed.

Figure 6. - Concluded. Velocity profiles downstream of rotor (station II). (See table I for explanation of data points.)

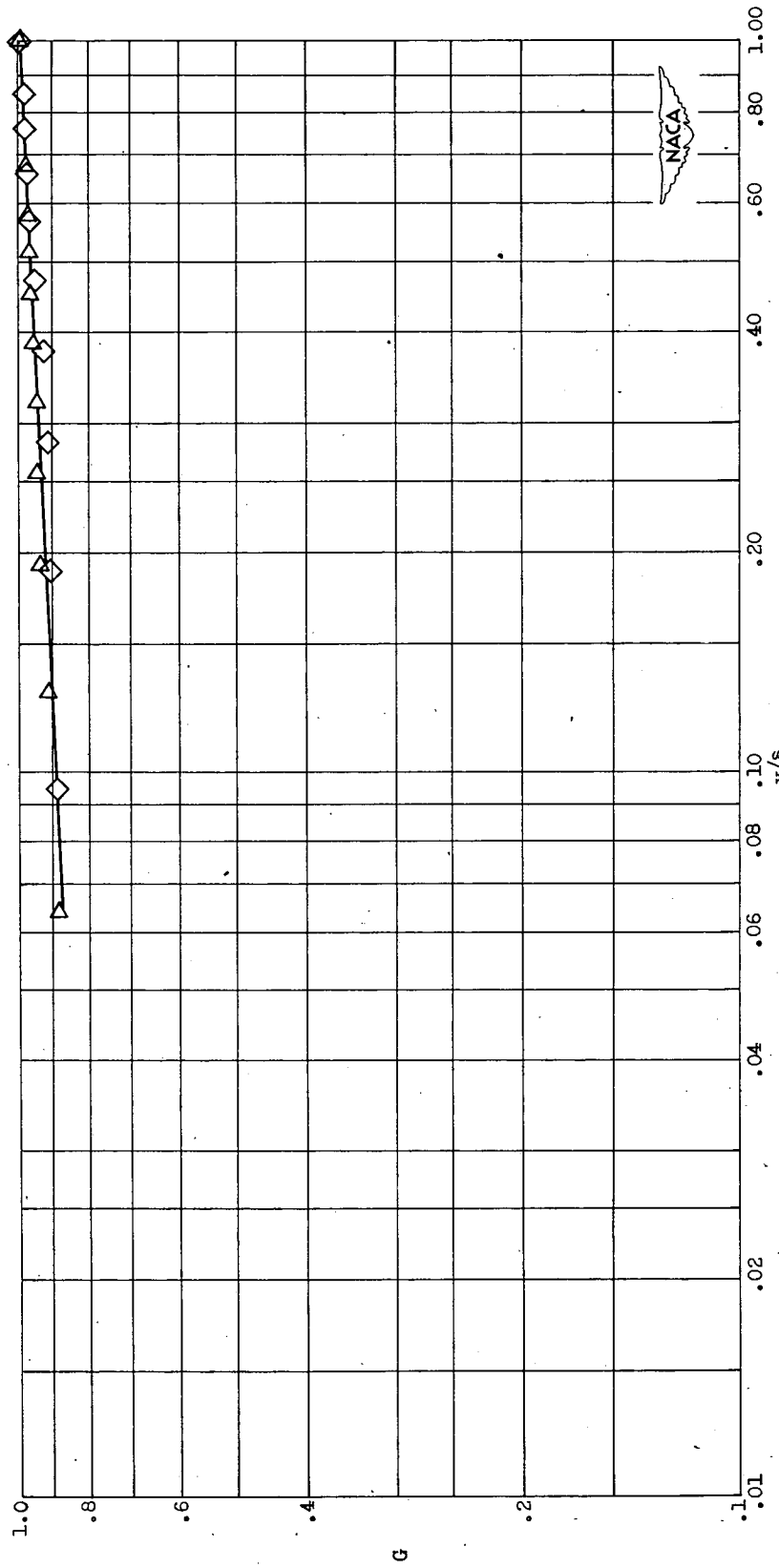


(a) Function G; no spoiler; 60 percent of design speed.

Figure 7. - Functions of G and g downstream of rotor (station II). (See table I for explanation of data points.)

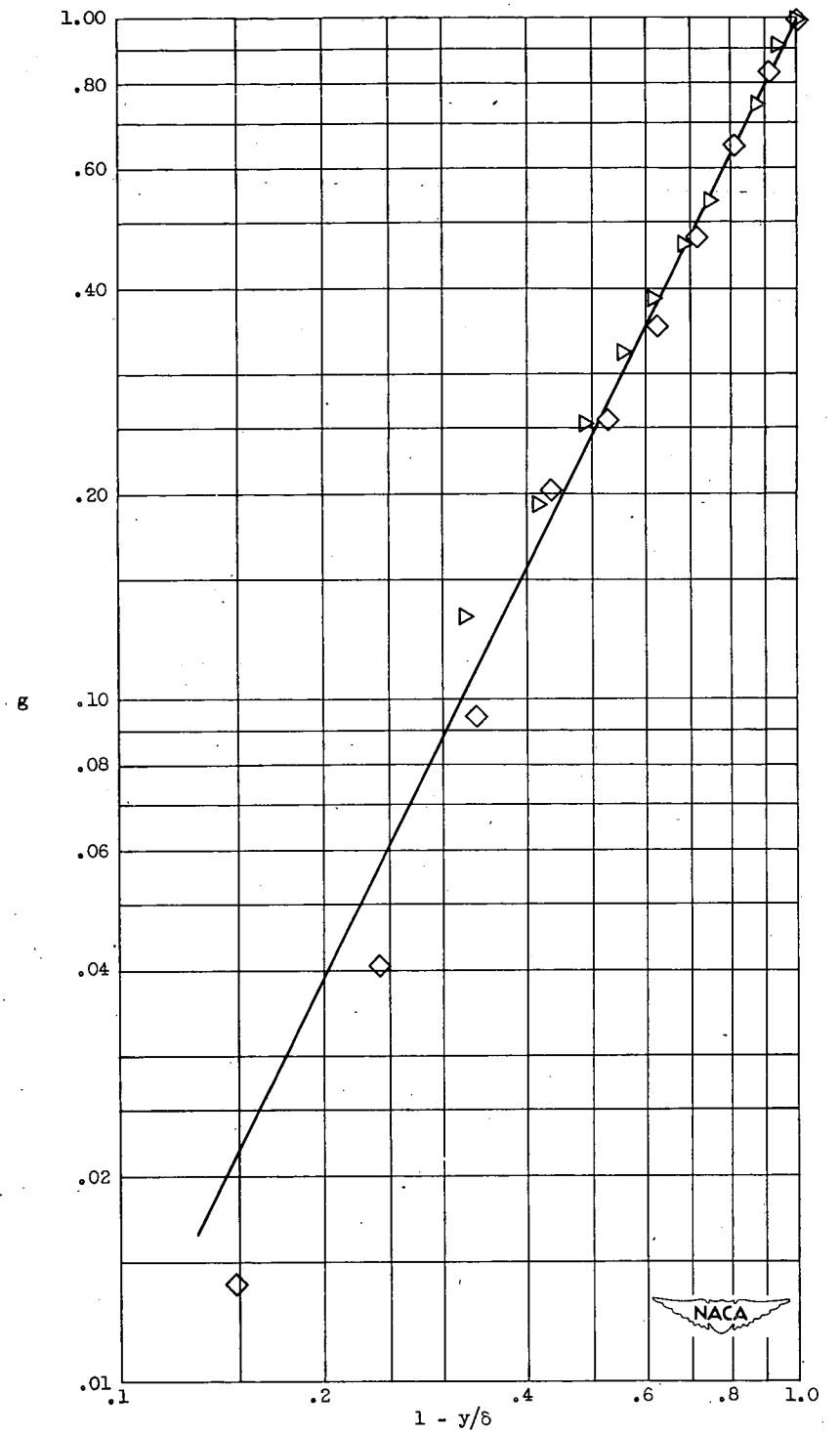


(b) Function g; no spoiler; 60 percent of design speed.

Figure 7. - Continued. Functions G and g downstream of rotor (station II). (See table I for explanation of data points.)

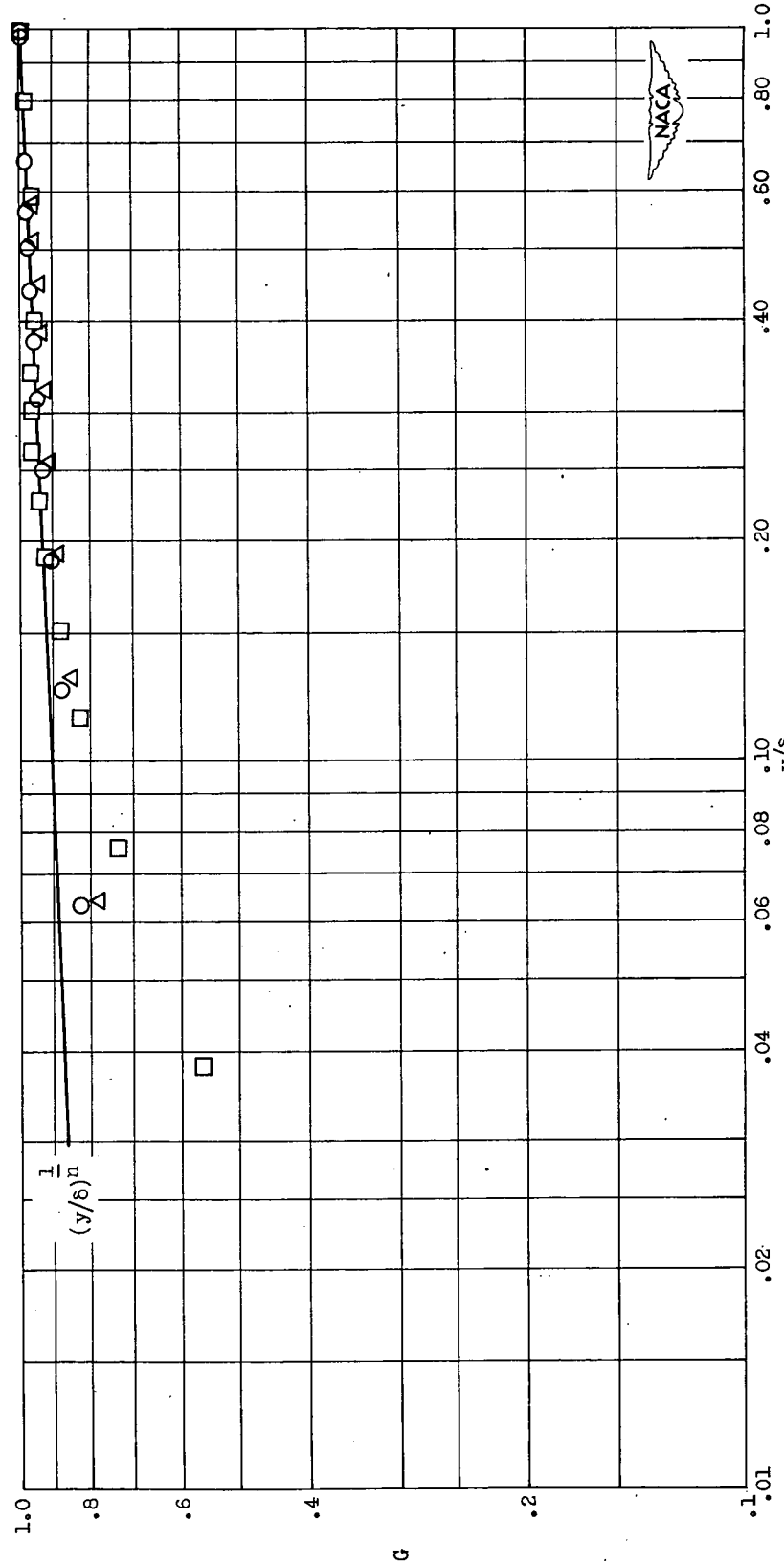


(c) Function G; $\frac{1}{8}$-inch spoiler; design speed.

Figure 7. - Continued. Functions G and g downstream of rotor (station II). (See table I for explanation of data points.)

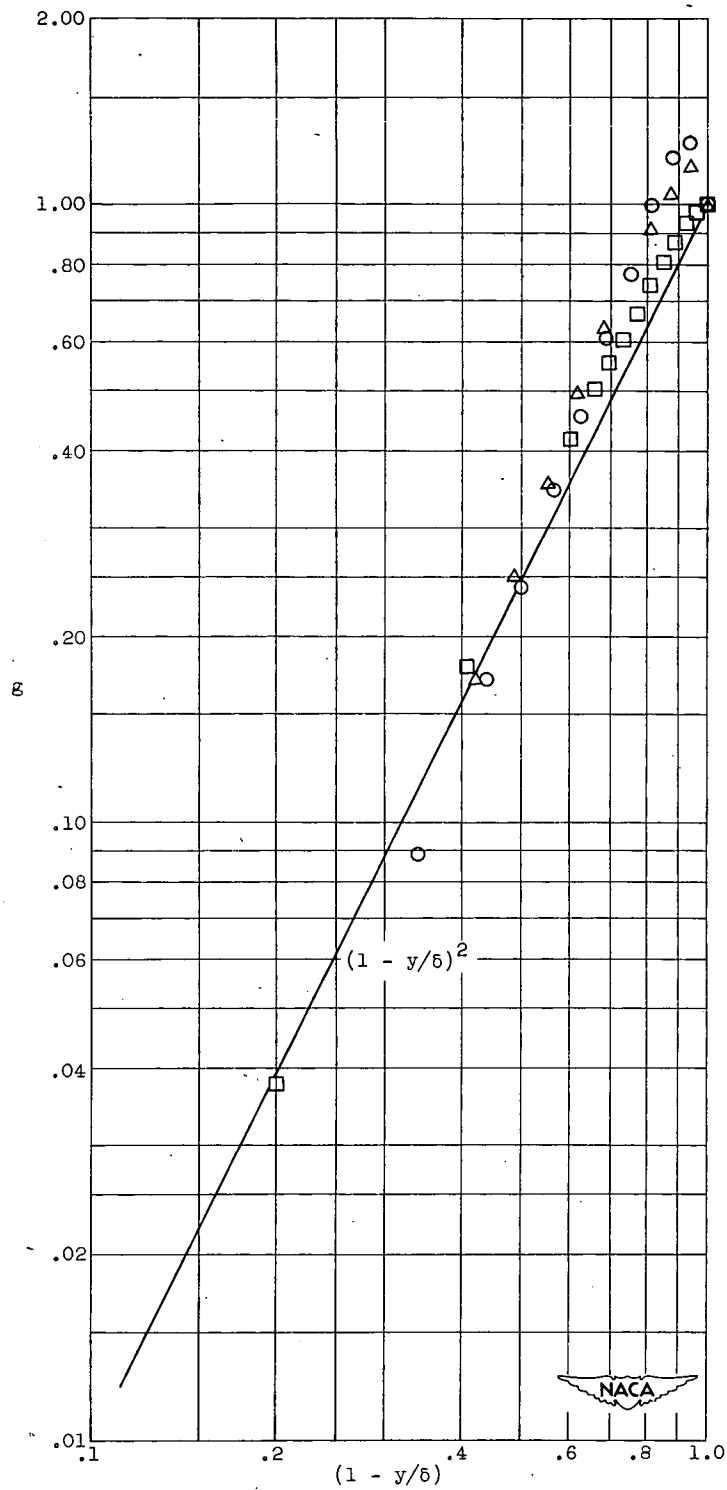


(d) Function g; $\frac{1}{8}$-inch spoiler; design speed.

Figure 7. - Continued. Functions G and g downstream of rotor (station II). (See table I for explanation of data points.)

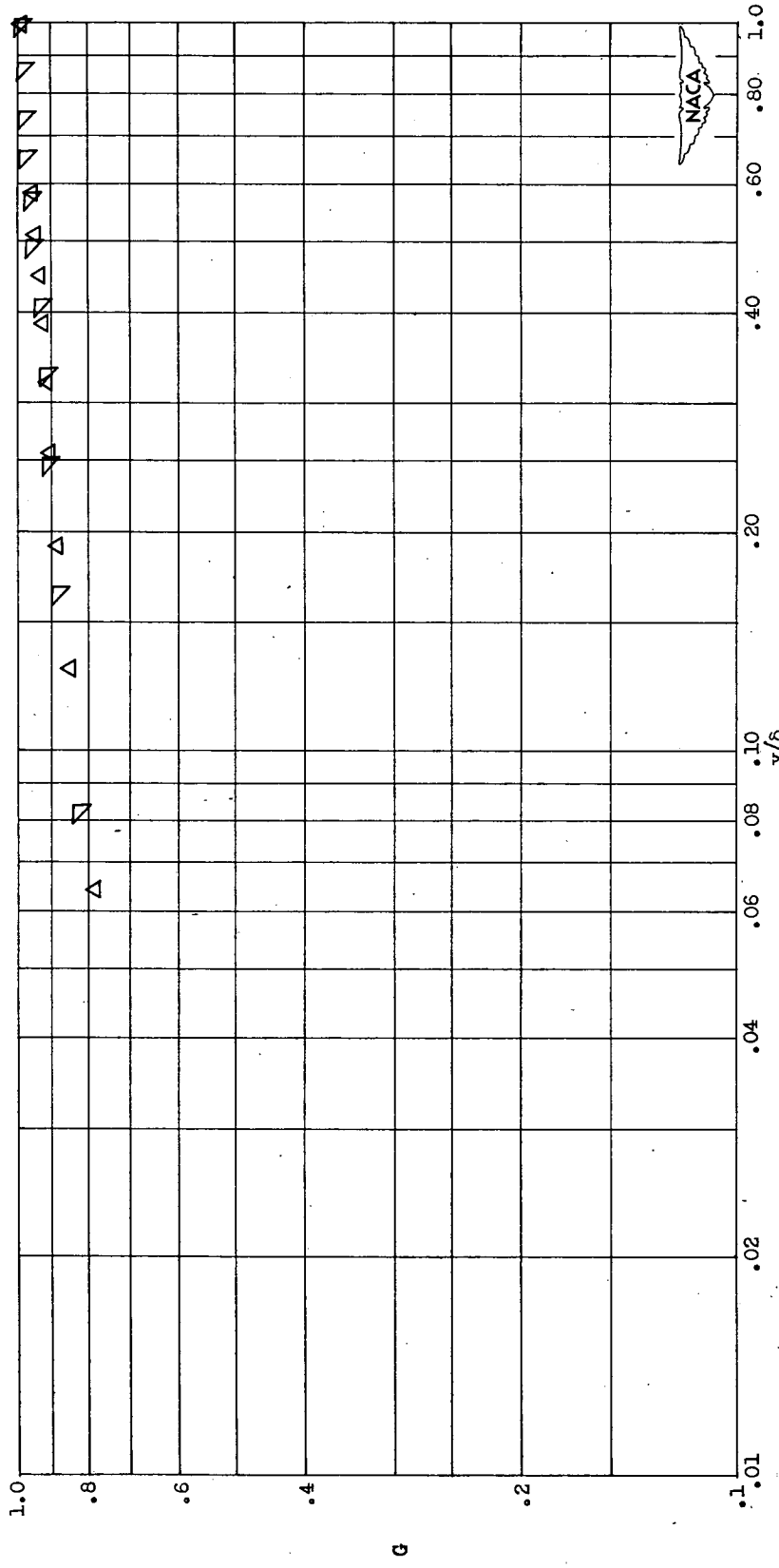


(e) Comparison of function G with and without spoiler; high weight flow; design speed.

Figure 7. - Continued. Functions G and g downstream of rotor (station II). (See table I for explanation of data points.)

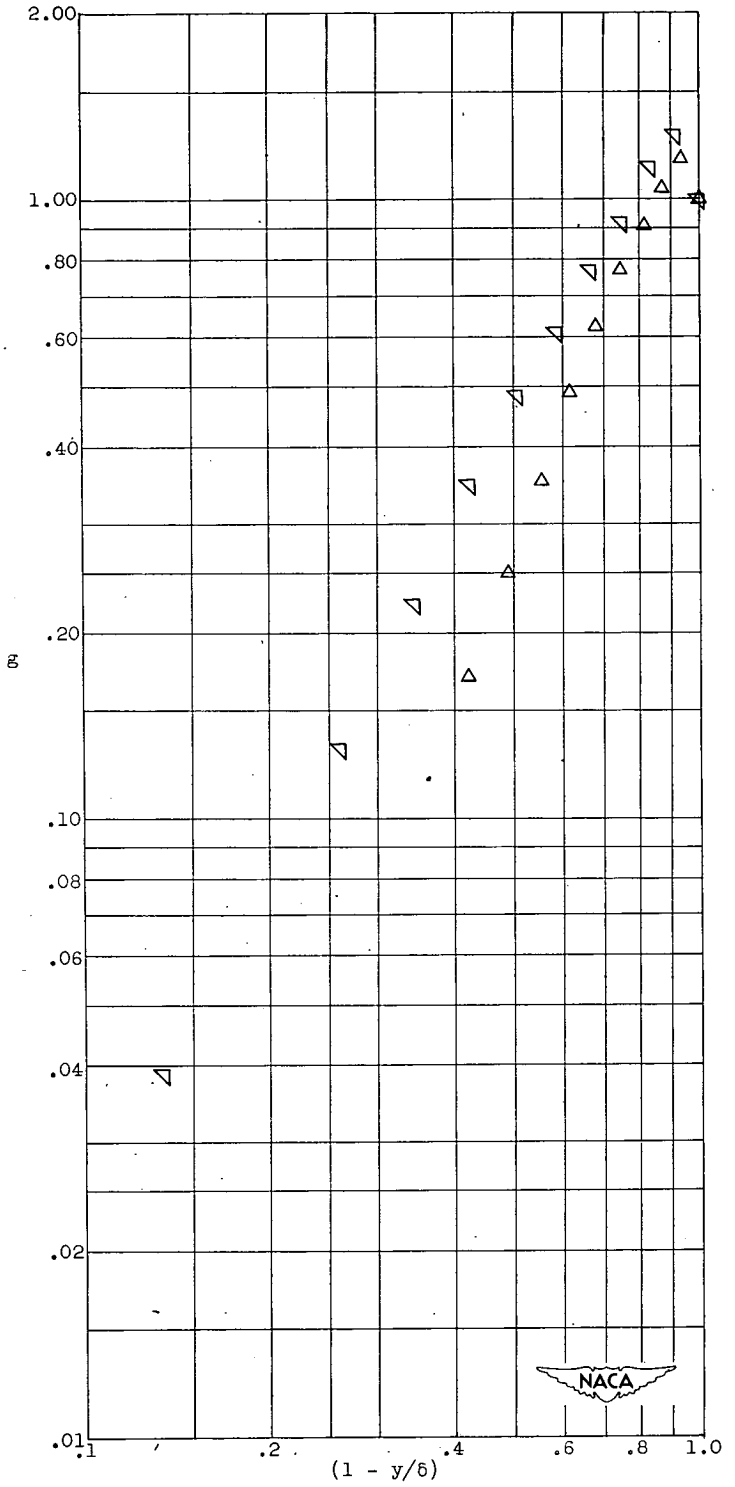


(f) Comparison of function g with and without spoiler; high weight flow; design speed.

Figure 7. - Continued. Functions G and g downstream of rotor (station II). (See table I for explanation of data points.)

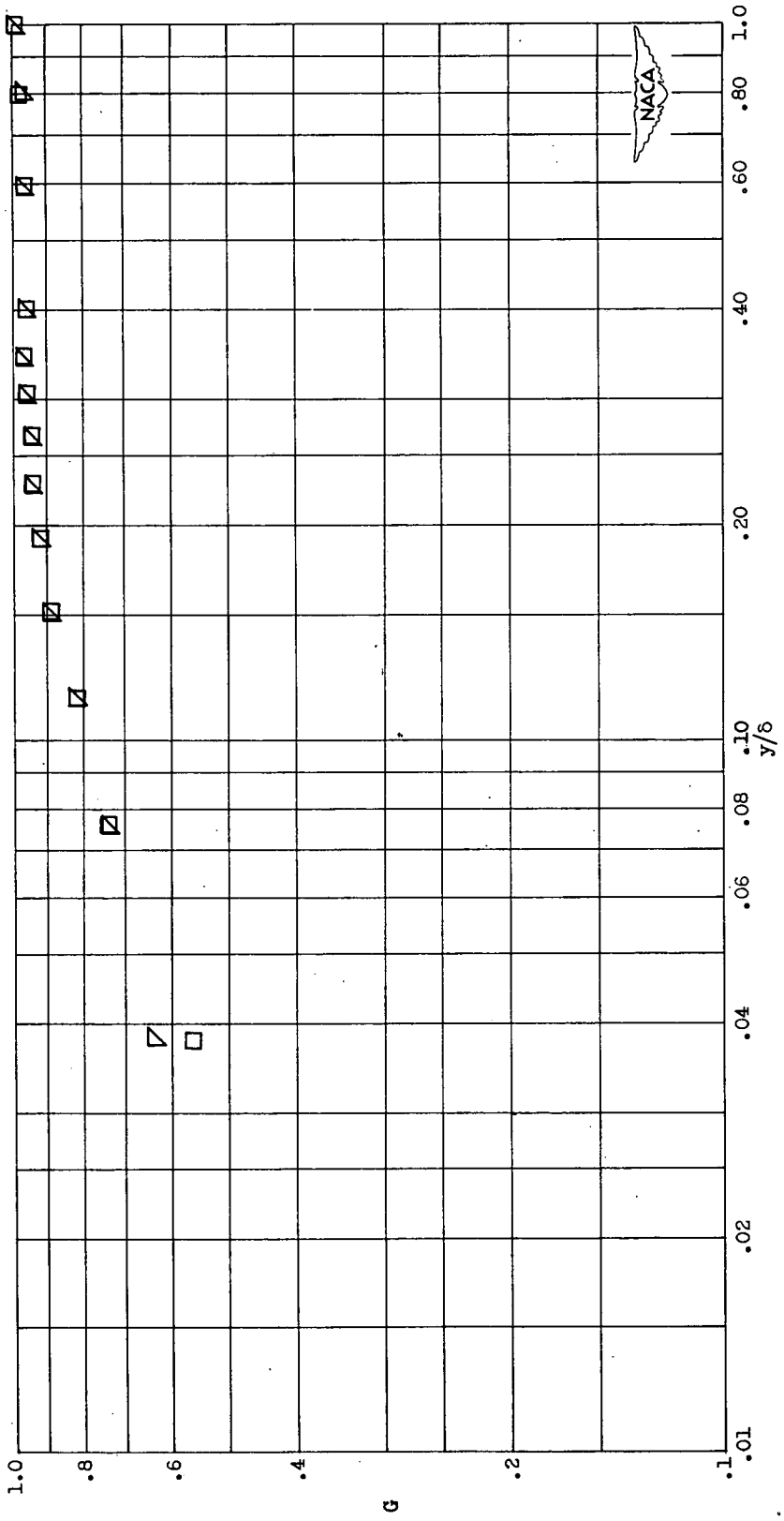


(g) Comparison of function G with and without spoiler; low weight flow; design speed.

Figure 7. - Continued. Functions G and g downstream of rotor (station II). (See table I for explanation of data points.)

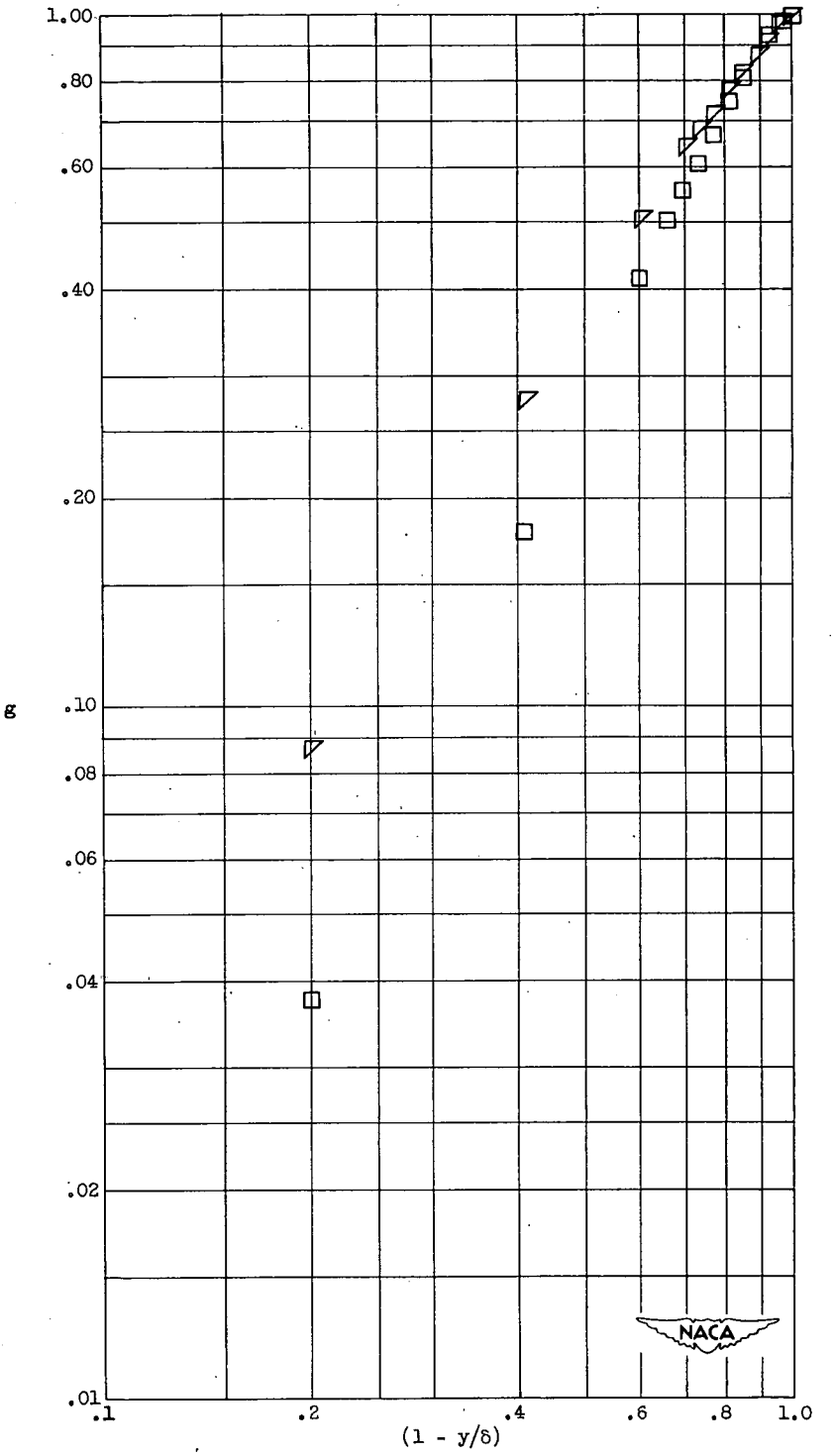


(h) Comparison of function g with and without spoiler; low weight flow; design speed.

Figure 7. - Concluded. Functions G and g downstream of rotor (station II). (See table I for explanation of data points.)

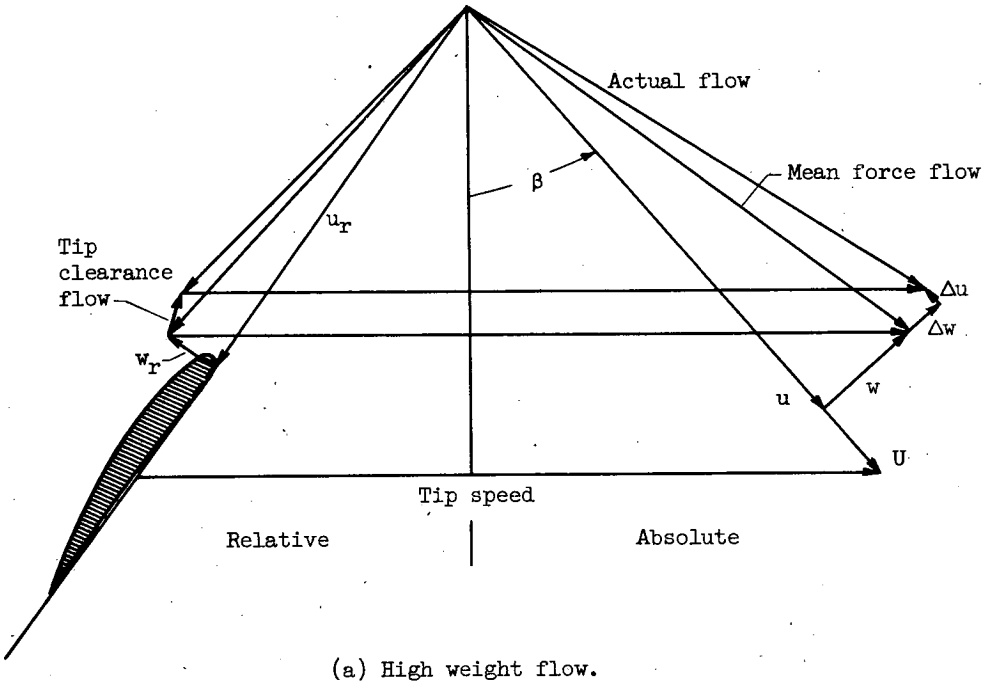


(a) High weight flow.

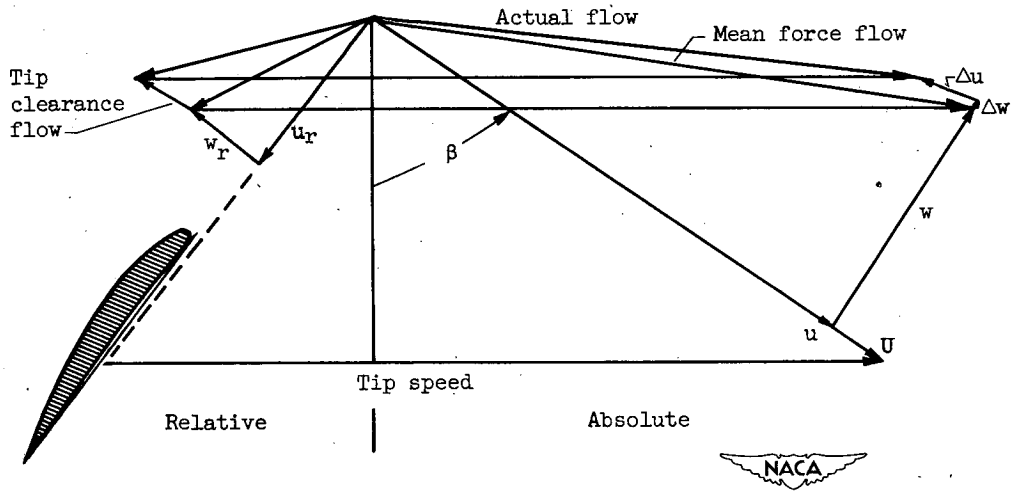


(b) Low weight flow.

Figure 8. - Velocity diagrams at $\frac{y}{\delta} = 0.10$. $\frac{1}{8}$-inch spoiler; design speed.

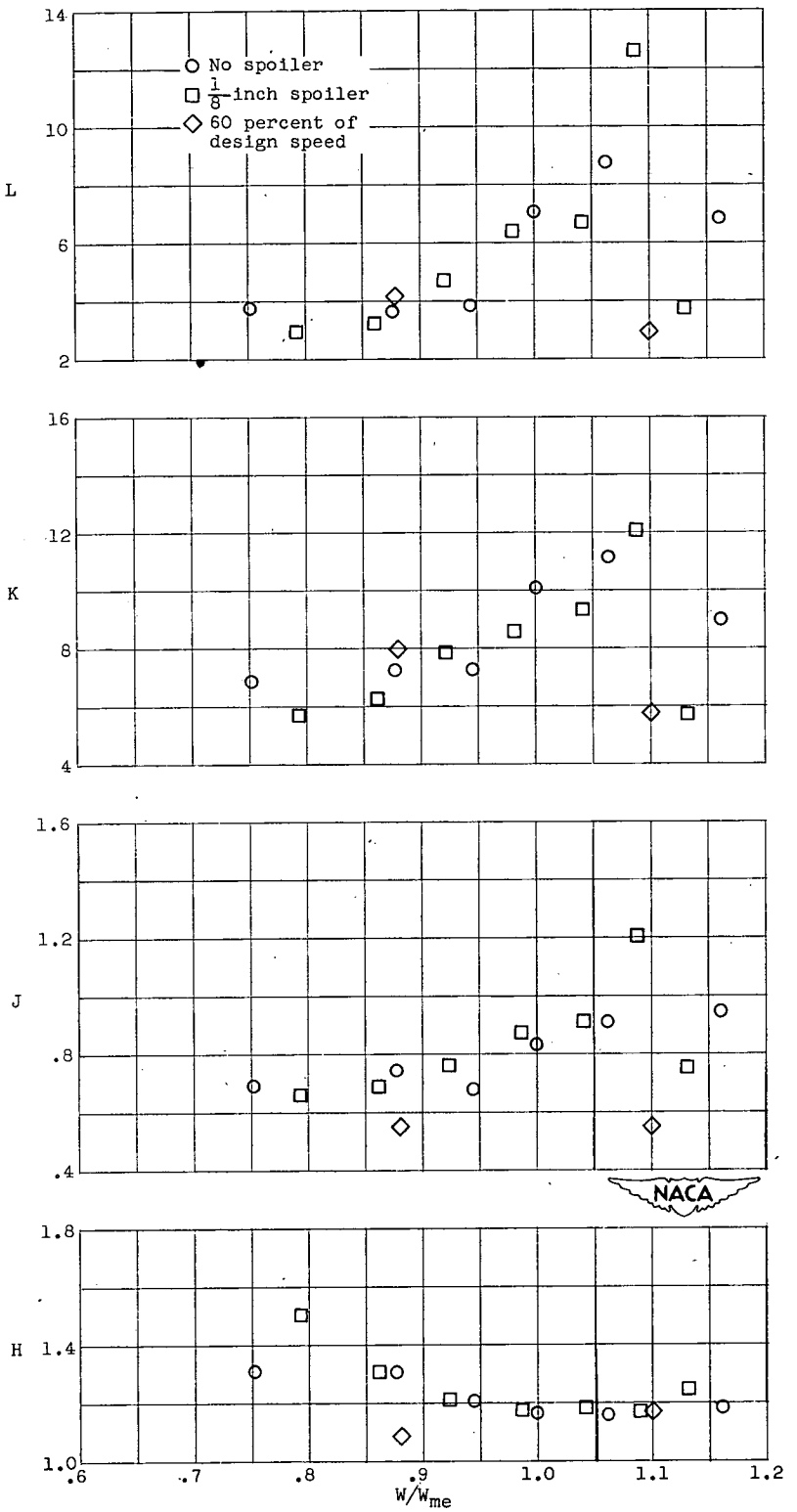


Figure 9. - Form factors H, K, J, L downstream of rotor (station II).

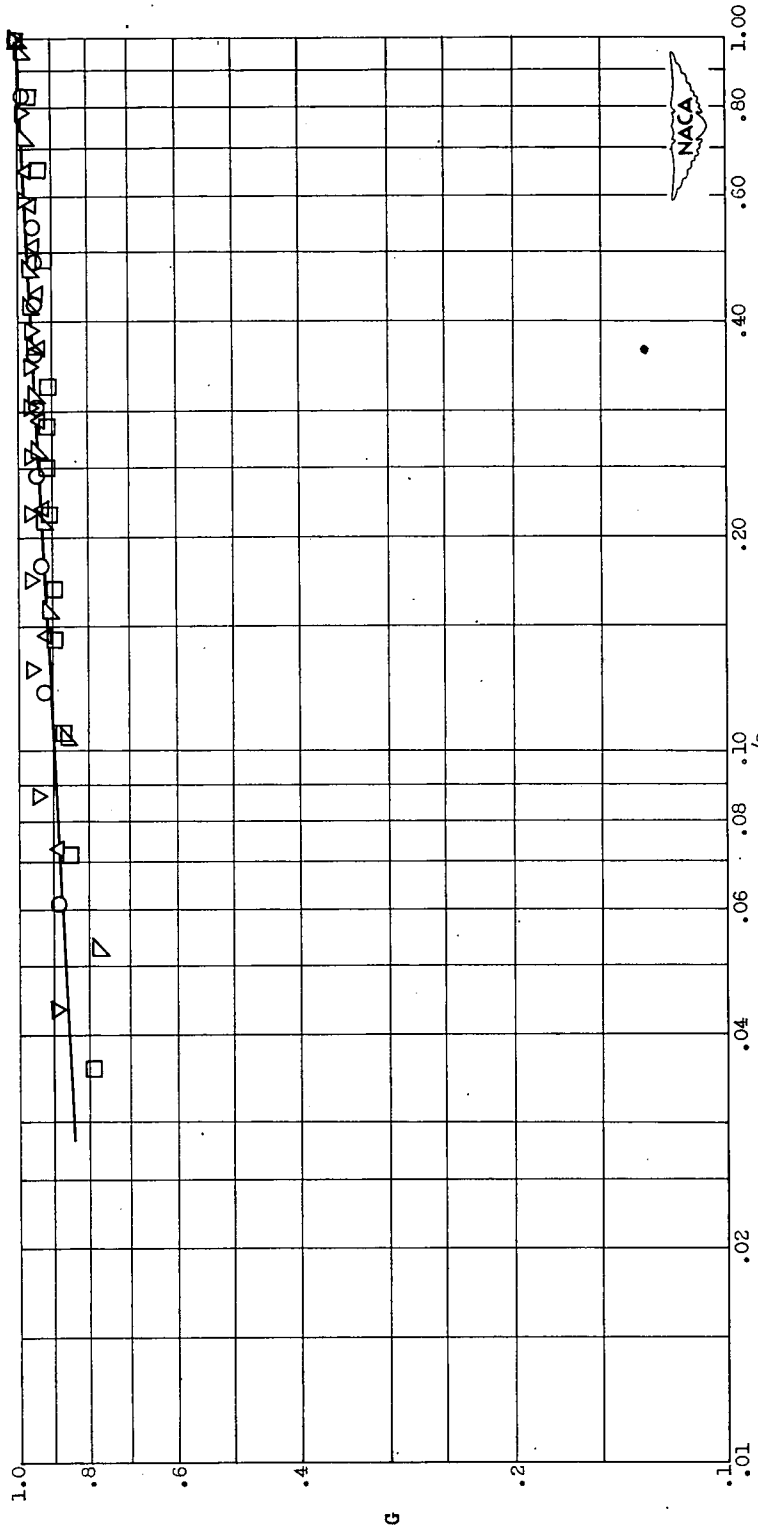


(a) Function G.

Figure 10. - Functions G and g at station III. (See table I for explanation of data points.)

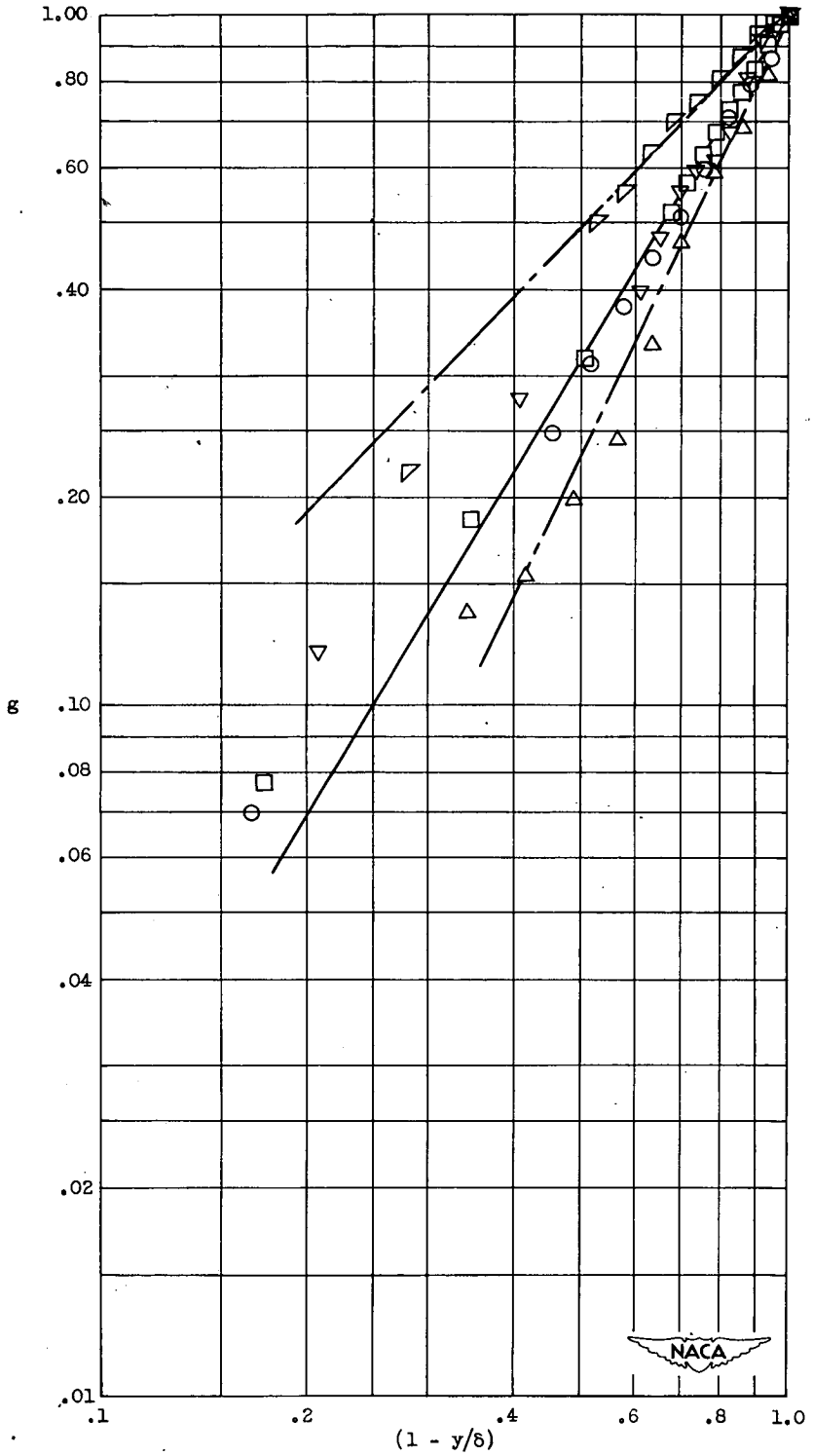


(b) Function g.

Figure 10. - Concluded. Functions G and g at station III.
(See table I for explanation of data points.)

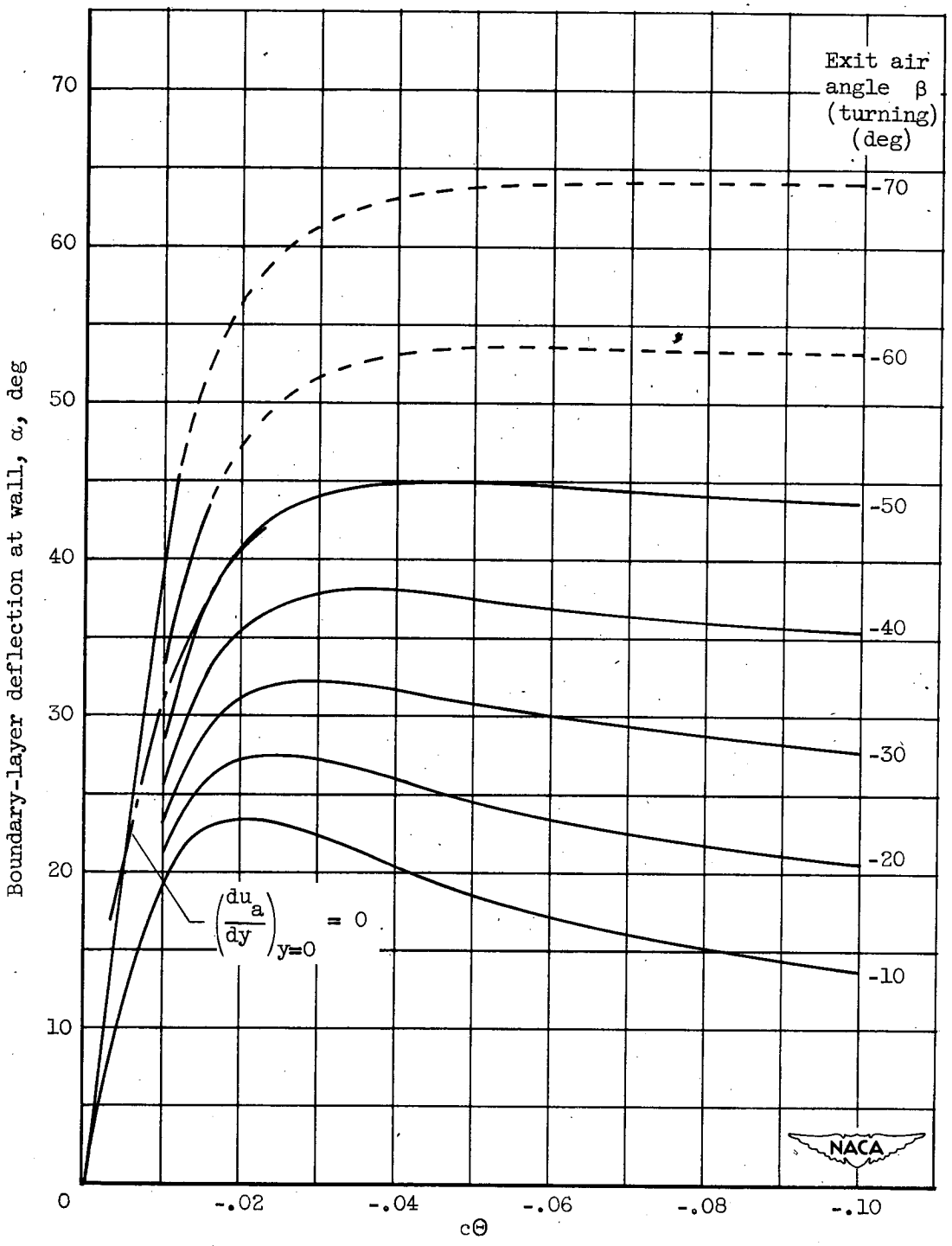


(a) Boundary-layer deflection angle at wall for constant turning.

Figure 11. - Approximate solution for boundary-layer deflection. U cos $\beta = U_o$; $\beta_o = 0$.

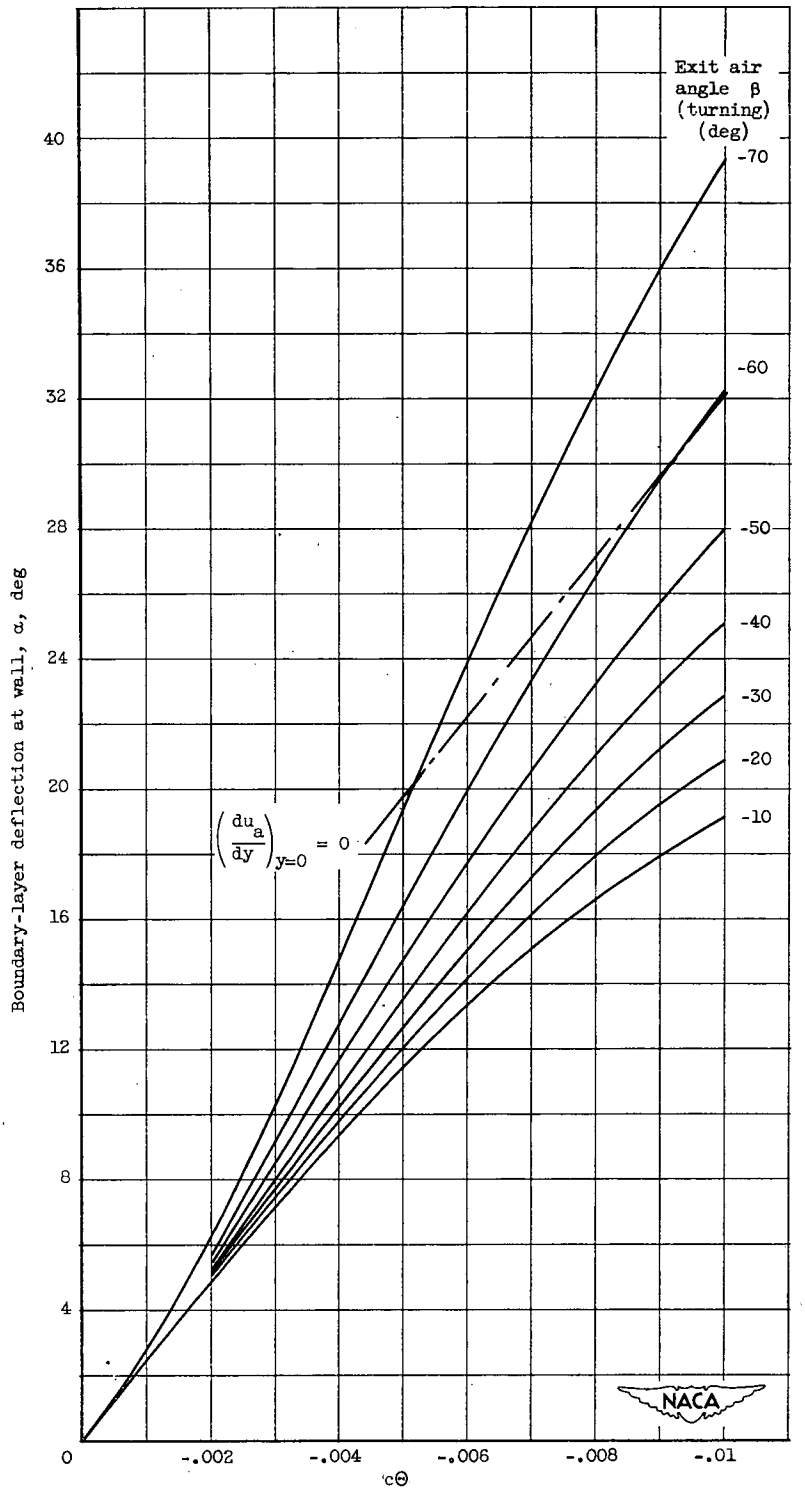


(b) Boundary-layer deflection angle at wall for constant turning. (Detail for $c\Theta > -0.01$.)

Figure 11. - Continued. Approximate solution for boundary-layer deflection. $U \cos \beta = U_o$; $\beta_o = 0$.

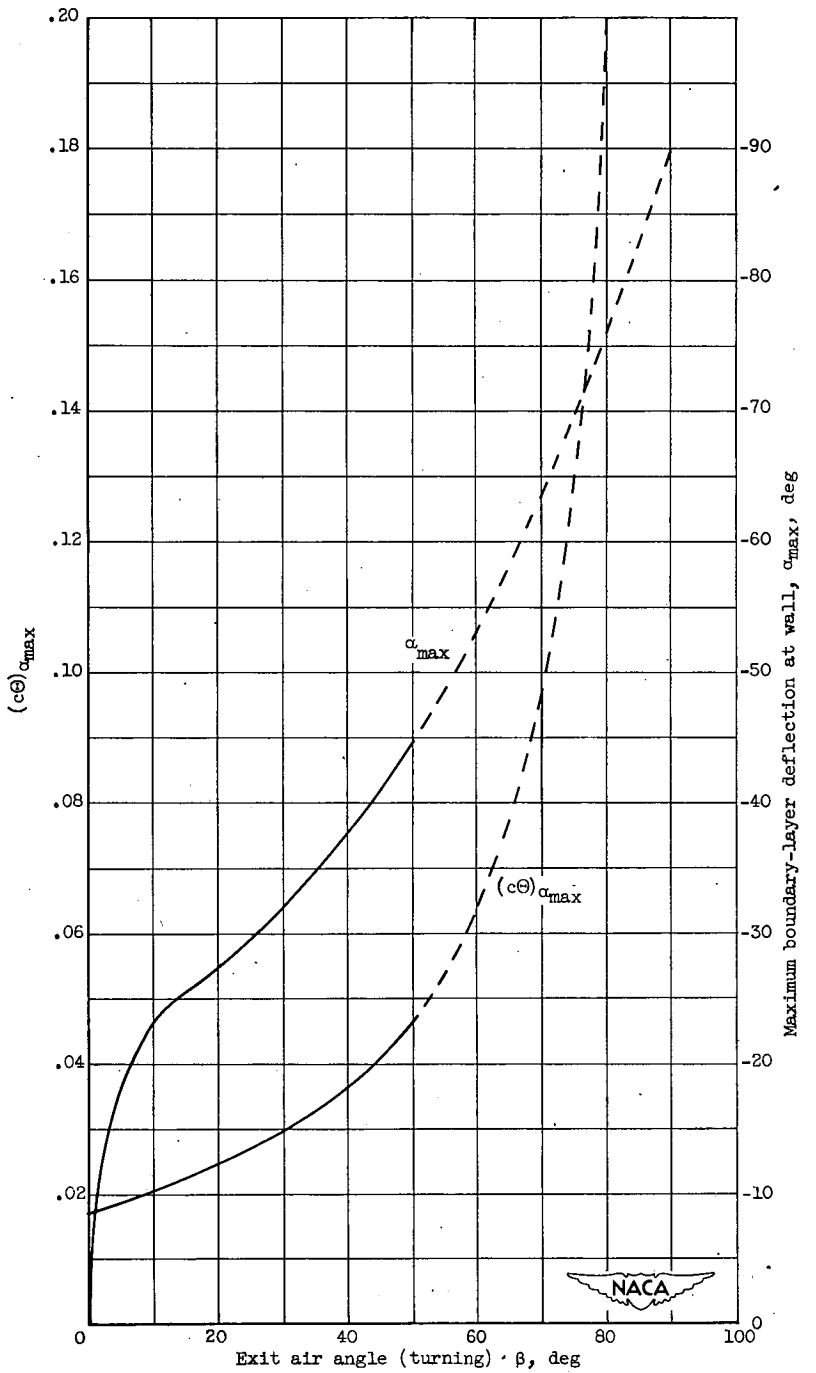


(c) Maximum boundary-layer deflection at wall for constant $c\Theta$.

Figure 11. - Concluded. Approximate solution for boundary-layer deflection. U cos $\beta = U_o$; $\beta_o = 0$.

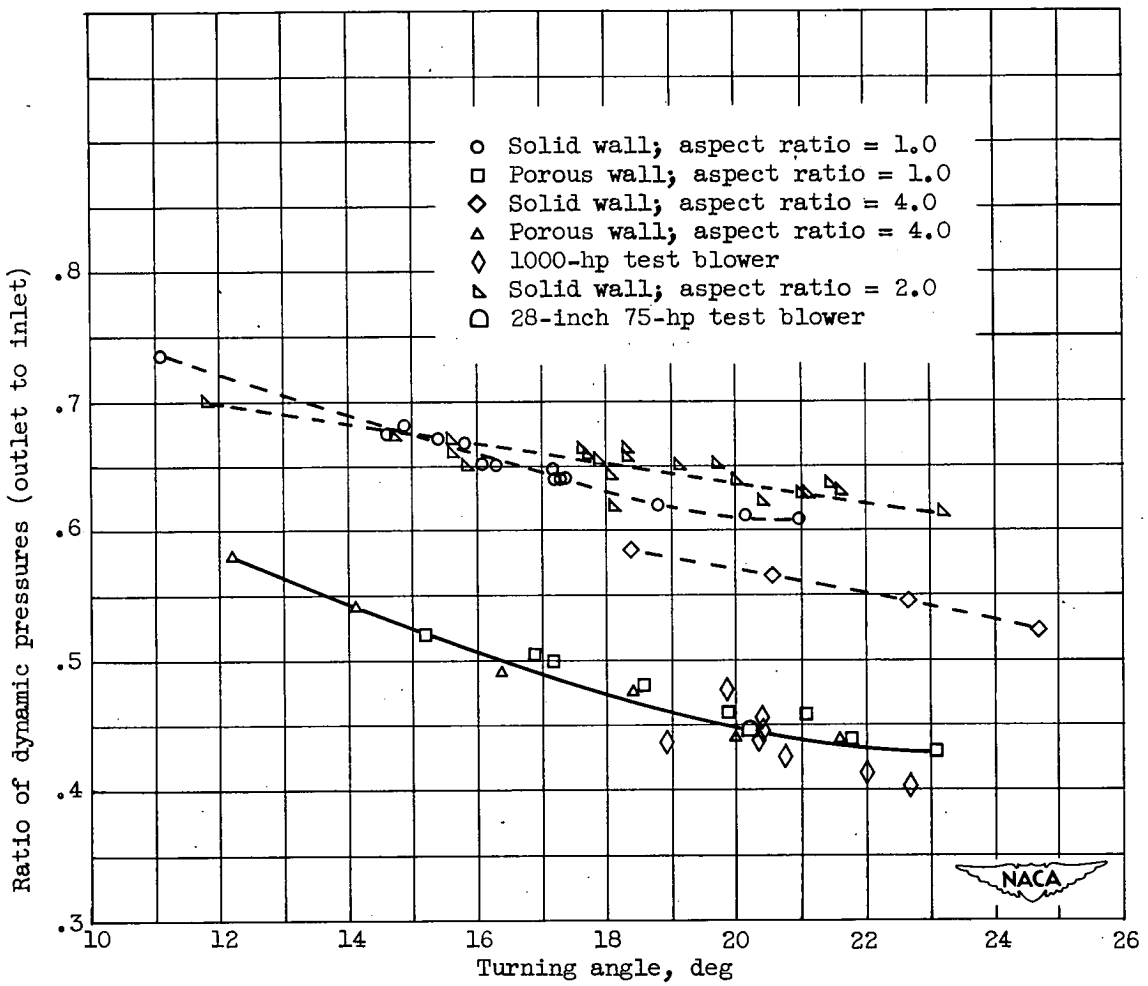


Figure 12. - Dynamic pressure ratio as measured in the various tunnel configurations tested. (Fig. 12 of reference 13.)

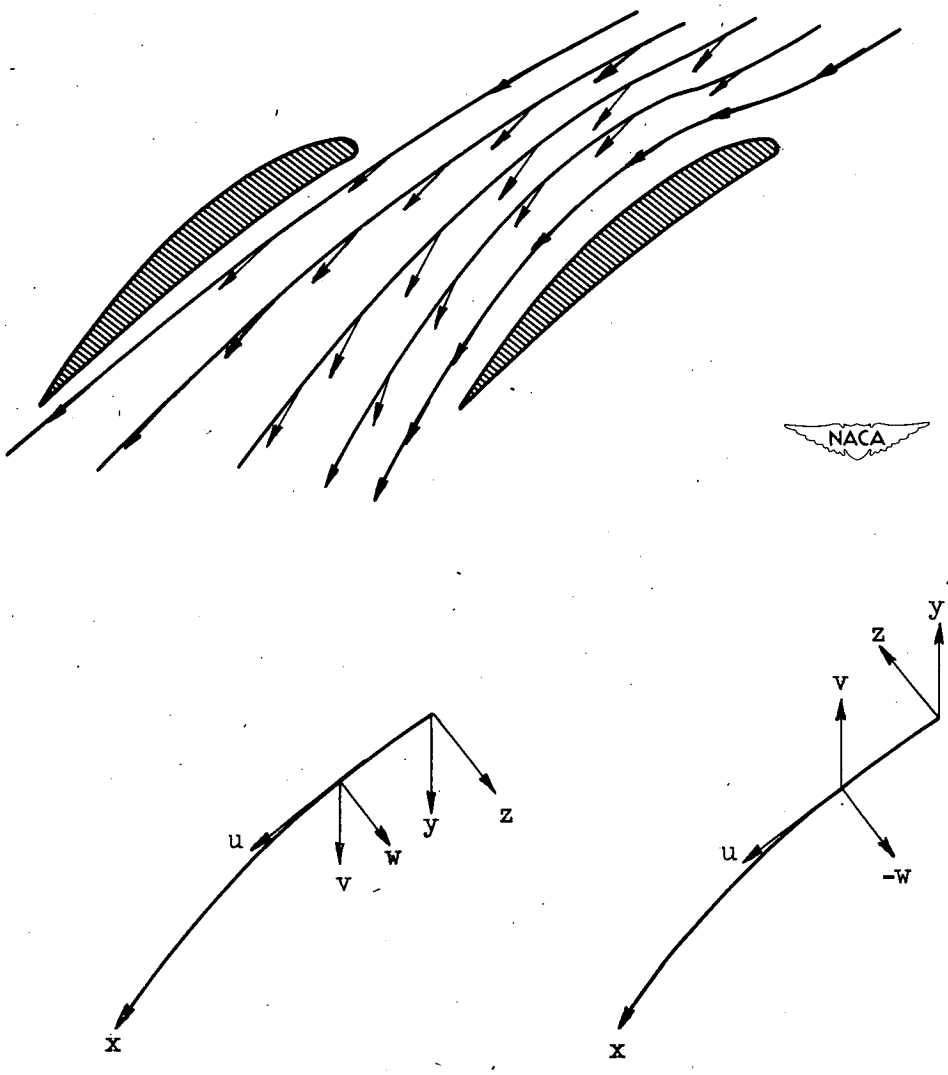


Figure 13. - Picture of flow and coordinate systems in guide vanes and cascades in boundary layer near wall.

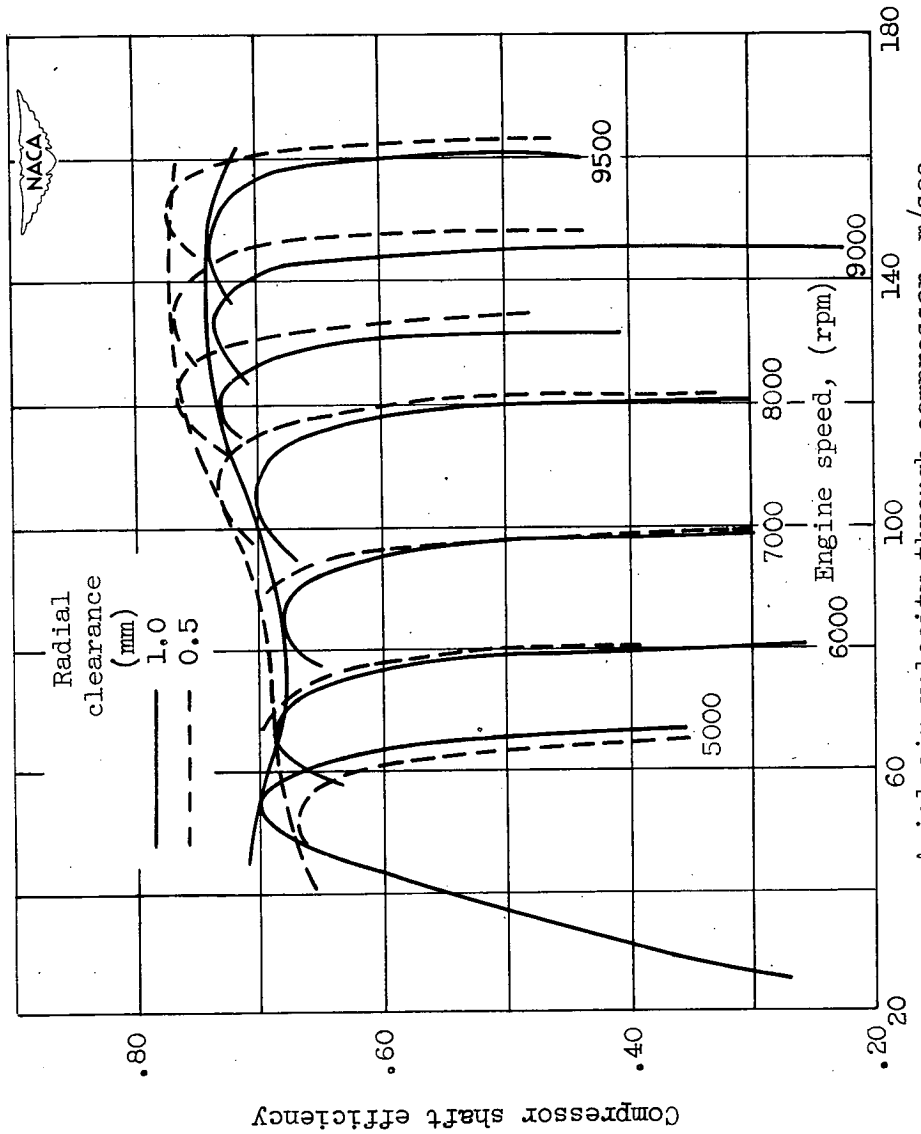


Figure 14. - Effect of radial clearance on compressor shaft efficiency. (Fig. 4 of reference 4.)

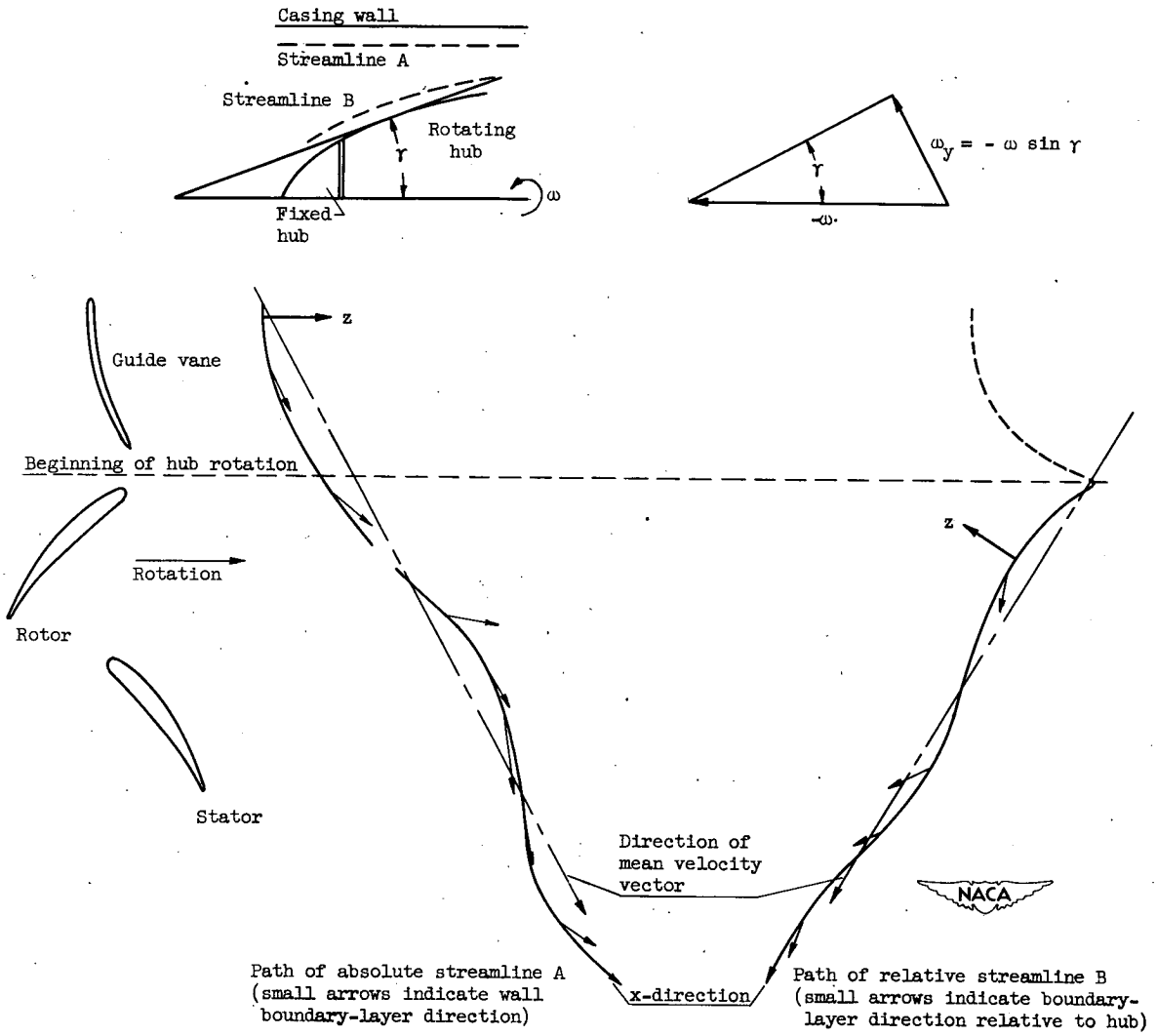


Figure 15. - Path of streamlines in compressor.

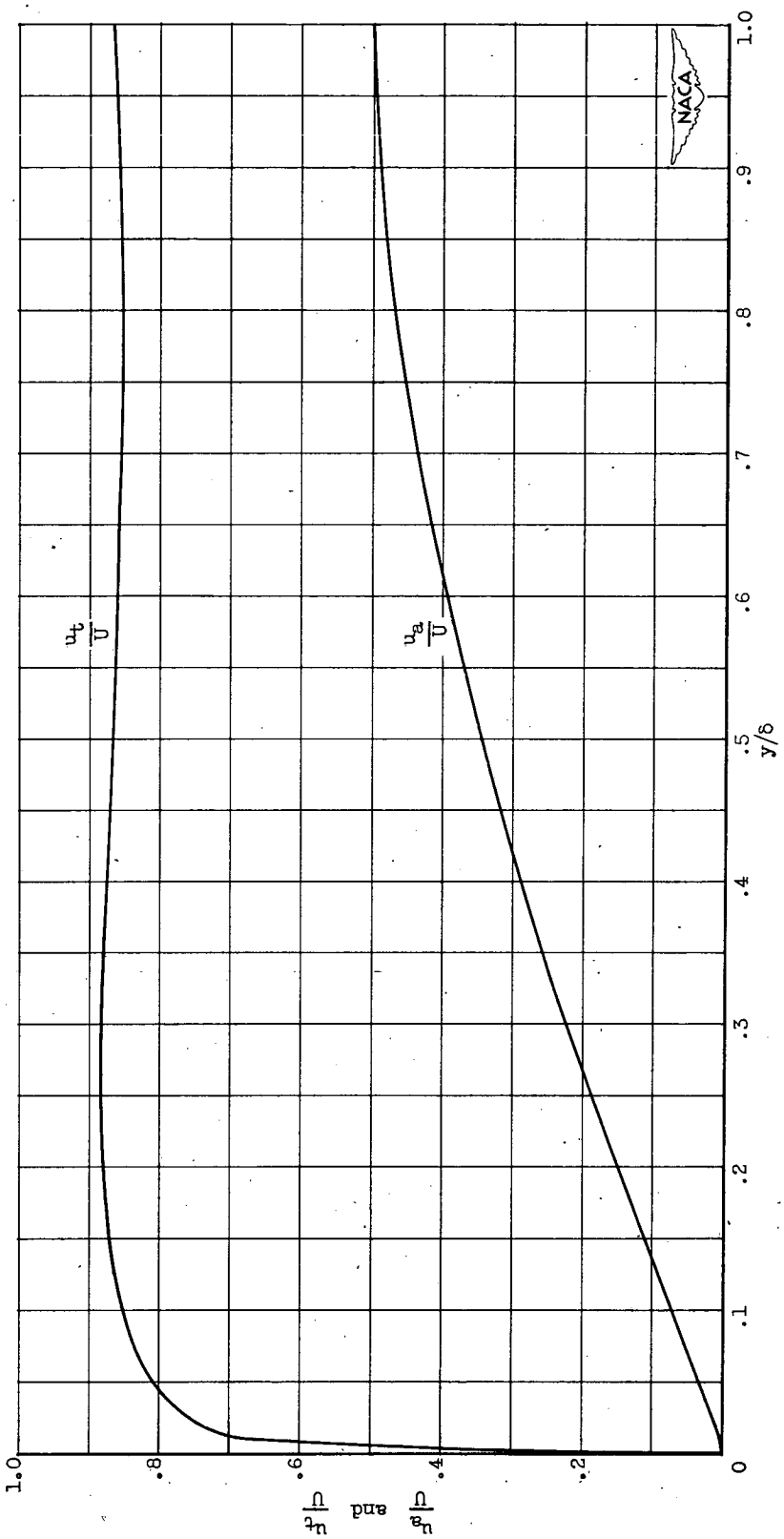


(a) $\alpha = 30^\circ$.

Figure 16. - Axial and tangential velocity profiles. $G = (y/\delta)^{\frac{1}{9}}$; $g = (1 - y/\delta)^2$; $\beta = -60^\circ$.

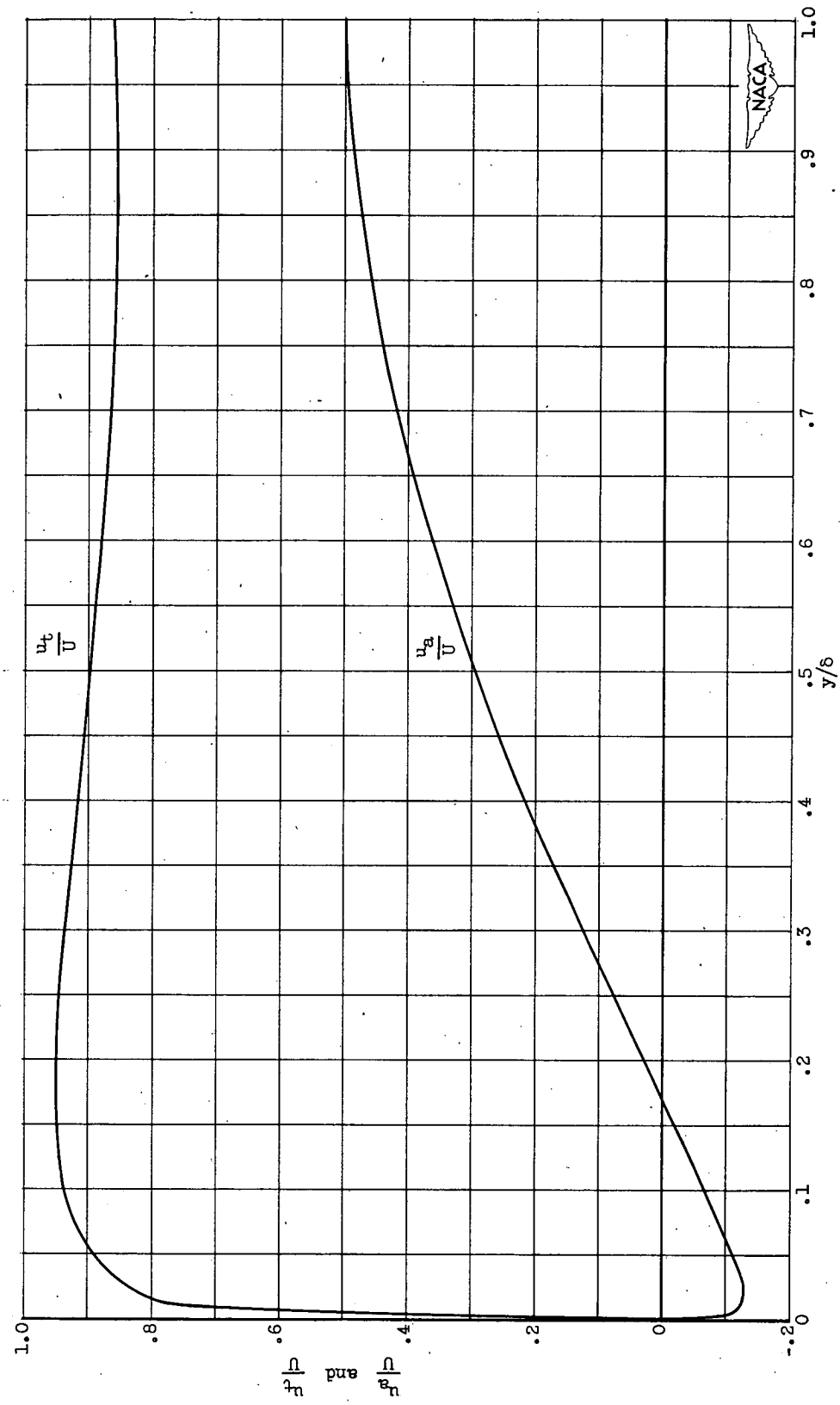


(b) $\alpha = 40^\circ$.

Figure 16. - Concluded. Axial and tangential velocity profiles. $G = (y/\delta)^{\frac{1}{9}}$; $g = (1 - y/\delta)^2$; $\beta = -60^\circ$.